Chemical Geology 344 (2013) 23–41

Contents lists available at SciVerse ScienceDirect

Chemical Geology

journal homepage: www.elsevier.com/locate/chemgeo

Late Neoarchean potassic high Ba–Sr granites in the Taishan granite–greenstone terrane: Petrogenesis and implications for continental crustal evolution

Touping Peng [a,b,*], Simon A. Wilde [b], Weiming Fan [a], Bingxia Peng [a]

[a] State Key Laboratory of Isotope Geochemistry, Guangzhou Institute of Geochemistry, Chinese Academy of Sciences, Guangzhou 510640, People's Republic of China
[b] Department of Applied Geology, Curtin University, PO Box U1987, Perth, Western Australia 6845, Australia

ARTICLE INFO

Article history:
Received 7 December 2012
Received in revised form 14 February 2013
Accepted 15 February 2013
Available online 24 February 2013

Editor: K. Mezger

Keywords:
Late Neoarchean
High Ba–Sr granite
Enriched mantle
Crustal evolution
Taishan granite–greenstone terrane
North China Craton

ABSTRACT

A series of Late Neoarchean high Ba–Sr granites with a potassium-rich signature has been identified from the Taishan granite–greenstone terrane (TSGT), within the Eastern Block of the North China Craton (NCC). LA-ICP-MS zircon dating shows that the Wanghailou, Hujiazhuang and Xiajiazhuang granitic intrusions were emplaced at ~2.54 Ga, ~2.52 Ga and ~2.47 Ga, respectively. Geochemically, they are alkali-rich, with high K_2O contents and high K_2O/Na_2O ratios, revealing their high-potassium calc-alkaline nature. They are enriched in large ion lithophile elements (LILE) and light rare earth elements (LREE) relative to typical A-, I- and S-type granites, and show negative anomalies in HFSE (Nb, Ta, Ti) and weak Eu anomalies. Their geochemical and isotopic characteristics, such as extremely low Y and Yb concentrations, high Sr/Y and $(La/Yb)_{cn}$ ratios, strongly fractionated REE patterns and elevated $\varepsilon_{Nd}(t)$ and $\varepsilon_{Hf}(t)$, imply that the parental magmas were derived directly from partial melting of the sub-arc enriched mantle at depths >15 kbar with residual garnet in the source. This mantle was previously depleted lithospheric mantle and was subsequently metasomatized by subduction-related fluids and/or melts. Fractional crystallization and crustal assimilation of these magmas during ascent resulted in their variable geochemical and isotopic characteristics. Taking into account the space–time patterns of late Archean magmatism in the area, an active subduction regime is favored to account for the generation of these potassic high Ba–Sr granites in the TSGT.

The two-stage Nd and Hf model ages of these granites suggest that continental crust older than 2.80 Ga is preserved beneath the TSGT. In combination with previous data from the region, it is noted that, apart from rapid crustal growth at ~2.7 Ga, other additions of mantle-derived magma, such as minor 2.6–2.5 Ga sanukitoids, siliceous high-Mg basalts (SHMBs) and high Ba–Sr granites, also made a significant contribution to continental crustal evolution in the TSGT.

1. Introduction

Granitic rocks are the main components of continental crust and are widely viewed as the end-products of growth of the Earth's lithosphere, either directly from mantle-derived magmas or by re-melting of pre-existing crust (e.g., Chappell and White, 1992; Rapp and Watson, 1995; Petford and Atherton, 1996; Chappell and White, 2001; Hawkesworth and Kemp, 2006a,b,c; Kemp et al., 2006, 2007). Due to differences in their origin, source and evolution, they display great diversity and thus can be used as indicators of geodynamic environments and, in some cases, as tracers of geodynamic evolution (Barbarin, 1999), especially now that the amount of data is so voluminous (e.g., Condie, 2000; Kemp and Hawkesworth, 2003; Souza et al., 2007; Kemp et al., 2009; Chebeu et al., 2011, and references therein). Probing the origin, transport and emplacement of granitoids is thus crucial for understanding continental crustal growth and crustal evolution. With approximately 70% of continental crust generated before the end of the Archean (e.g., Hawkesworth and Kemp, 2006a; Kemp et al., 2007): much of this consists of Na-rich tonalite–trondhjemite–granodiorite (TTG), with minor potassium-rich granitoids (e.g., Sylvester, 1994). These Archean Na-rich TTG and potassium-rich granitic rocks are characterized by high Ba–Sr contents (Ba > 500 ppm and Sr > 300 ppm) and strongly fractionated REE patterns, similar to the Phanerozoic high Ba–Sr granites, such as those from the Silurian (Caledonian), Late Cretaceous and Tertiary orogenic belts worldwide (e.g., Tarney and Jones, 1994; Qian et al., 2003; Fowler et al., 2008; Ye et al., 2008; Choi et al., 2009). Such signatures are different from the typical Phanerozoic granitic rocks that have commonly been classified into I-, S- and A-type granites, with low Ba–Sr contents and only moderately fractionated REE patterns (e.g., Chappell and White, 1992; Frost et al., 2001 and references therein). In general within a given terrane, potassium-rich

* Corresponding author at: Guangzhou Institute of Geochemistry, Chinese Academy of Sciences, P.O. Box 1131, Guangzhou 510640, People's Republic of China. Tel.: +86 20 85292410; fax: +86 20 85291510.
E-mail address: tppeng08@126.com (T. Peng).

0009-2541/$ – see front matter © 2013 Elsevier B.V. All rights reserved.
http://dx.doi.org/10.1016/j.chemgeo.2013.02.012

granitoids typically follow emplacement of Na-rich TTG, and formed mainly at the Archean–Proterozoic boundary (e.g., Jayananda et al., 1995; Frost et al., 1998; Jayananda et al., 2000; Moyen et al., 2001, 2003). Although these potassic granitic rocks are only a minor component of Archean granite–greenstone terranes, they nonetheless comprise a significant part of the Archean crust (Sutcliffe et al., 1990) and have a disproportionate tectonic importance. Studies have demonstrated that most of the late potassic granitoids, especially the sanukitoids and the Closepet-type granites (e.g., Frost et al., 1998; Jayananda et al., 2000; Smithies and Champion, 2000; Moyen et al., 2001, 2003; Halla, 2005; Lobach-Zhuchenko et al., 2005; de Oliveira et al., 2009; Martin et al., 2009; Moyen, 2011), originated directly from an enriched lithospheric mantle rather than by reworking (partial melting) of earlier TTG. Hence, these potassic high Ba–Sr granitoids carry important clues as to their source, petrogenesis and mechanisms of continental crustal formation and crustal evolution in the Archean (e.g., Taylor and McLennan, 1985; Rudnick, 1995).

The North China Craton (NCC) is composed of the Eastern and Western blocks, and the intervening Trans-North China Orogen (Fig. 1a; Zhao et al., 2001). The Eastern Block of the NCC contains the oldest rocks in China (~3.8 Ga) (e.g., Liu et al., 1992, 2008; Wilde et al., 2008) and underwent rapid crustal growth at around 2.7 Ga, similar to most other Archean cratons (e.g., Jahn et al., 1988; Cao et al., 1996; Wu et al., 2005b; Wan et al., 2010, 2011). Unlike other cratons, however, a strong tectono-magmatic event at ~2.5 Ga is recorded across the whole NCC (e.g., Zhao et al., 2005; Yang et al., 2008; Wan et al., 2010, 2012c). Thus, ~2.5 Ga igneous rocks predominate and only minor ~2.7 Ga granites and greenstones are present, mostly occurring in the Eastern Block (Wan et al., 2010, 2011, 2012a and references therein). The ~2.7 Ga granitoids are dominantly Na-rich TTGs, with subordinate potassic granitoids and high-Mg rocks (e.g., Polat et al., 2006; Wang et al., 2009; Wan et al., 2010, 2012c). From field and geochronological evidence, the potassium-rich granitic rocks in the NCC also post-date the Na-rich TTG. Several show an affinity to high Ba–Sr granite (Yang et al., 2008). These potassic high Ba–Sr granites record important information on the growth and evolution of continental crust in the Eastern Block of the NCC, particularly in the TSGT where typical greenstones crop out (e.g., Zhao et al., 2001; Polat et al., 2006). In this contribution, we present new geochronological, elemental and whole-rock Nd and zircon Hf isotopic data for the late Neoarchean potassic high Ba–Sr granites in the TSGT. Our aims are to: (1) characterize the petrogenesis of these potassium-rich granites and the nature of their source; (2) provide an insight into the tectonic setting, and (3) advance our understanding of the mode of continental crustal growth in the Archean.

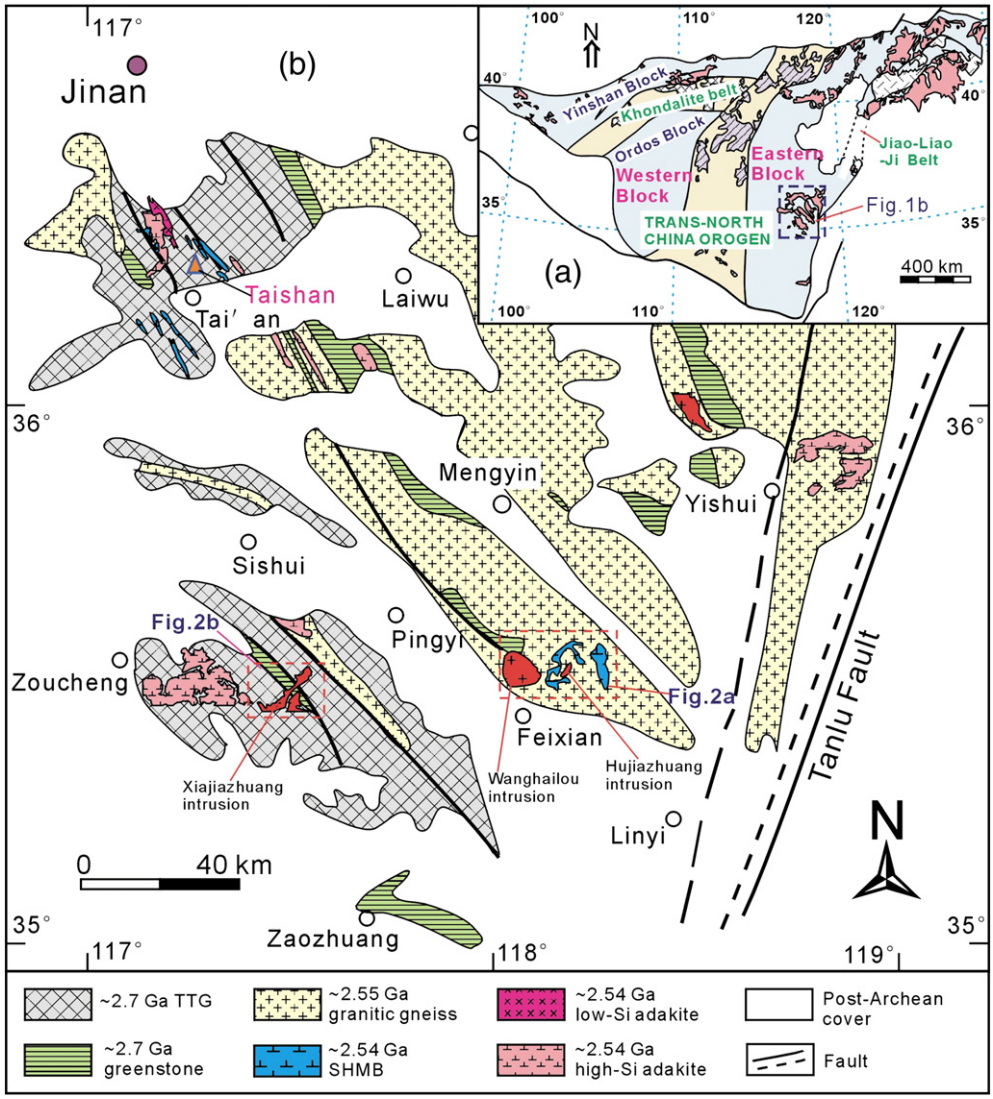

Fig. 1. (a) Tectonic subdivision of the North China Craton (modified from Zhao et al., 2005). (b) Simplified geological map of the TSGT (modified after Wan et al., 2010). SHMB = siliceous high-Mg basalt.

2. Geological setting and petrography

The North China Craton formed by the amalgamation of the Eastern and Western Blocks along the Trans-North China Orogen at ~1.85 Ga (Fig. 1a; Zhao et al., 1999a,b, 2000, 2001, 2005; Kröner et al., 2006; Liu et al., 2006; Zhang et al., 2006; Zhao et al., 2006; Trap et al., 2007; Zhang et al., 2007; Zhao et al., 2007, 2008a,b; Zhang et al., 2009). The Western Block is further subdivided into the Yinshan Block in the north and the Ordos Block in the south, which amalgamated along the Khondalite Belt at ~1.95 Ga (Fig. 1a; Zhao et al., 2003; Xia et al., 2006a, b, 2008, 2009; Yin et al., 2009; Zhao, 2009; Zhao et al., 2010; Zhou et al., 2010; Yin et al., 2011), whereas the Eastern Block experienced a rifting event at ~1.90 Ga and subsequent collision between the Longgang and Langrim Blocks, forming the Jiao-Liao-Ji Belt (Fig. 1a; Luo et al., 2004; Li et al., 2005, 2006; Li and Zhao, 2007; Luo et al., 2008; Zhou et al., 2008; Tam et al., 2011, 2012a,b). The Eastern Block is dominated by ~2.7–2.6 Ga TTG gneisses, mafic–ultramafic igneous rocks, ~2.52 Ga diorite, granodiorite, monzogranite, and K-feldspar granite plutons and syntectonic charnockites, with minor 2.55–2.50 Ga bimodal volcanics and sedimentary supracrustal rocks (Zhao et al., 1998, 2001; Wu et al., 2005a, 2008; Yang et al., 2008; Jiang et al., 2010; Li et al., 2010; Wan et al., 2010, 2011, 2012b, c). In addition, some granitoid intrusions with an age of 3.3–2.8 Ga had been recognized in the Eastern Block (Liu et al., 1992; Song et al., 1996). The oldest known basement within the craton is also located here, and has been dated at 3.8 Ga (Liu et al., 1992; Wu et al., 2005a,b; Liu et al., 2008; Nutman et al., 2011).

The TSGT is located in western Shandong Province within the Eastern Block of the NCC (Fig. 1a), with a total area of >10,000 km^2. It extends in a northwest–southeast direction, being truncated by the Tanlu Fault in the east (Fig. 1b). The basement gneisses are Mesoarchean to Paleoproterozoic in age, and are partially overlain by Paleoproterozoic to Cenozoic platform cover. Neoarchean basement rocks crop out widely and are dominantly ~2.7–2.5 Ga TTG gneisses and gneissic monzogranites, accounting for 80% of the total Precambrian basement in the TSGT (Jahn et al., 1988; Wan et al., 2010). Minor ~2.7–2.6 Ga ultramafic to felsic volcanic rocks and metasedimentary rocks occur as lenses within the TTG gneisses and constitute the Taishan greenstone belt (Fig. 1b; Xu et al., 1992; Cao et al., 1996). Recently, an additional younger igneous suite (~2.54 Ga), including enriched mantle-derived (previously depleted) magmas (i.e., sanukitoids and siliceous high-Mg basalts) and subducted slab-derived rocks (adakitic intrusions), has been identified (Wang et al., 2009; Peng et al., 2012, 2013). Field observations suggest that these later plutons intrude the TTG gneisses (Jahn et al., 1988; Cao et al., 1996; Wu et al., 1998), and were metamorphosed at lower grades than the gneissic country rocks. Also, diorites and granites with a similar emplacement age of ~2.54 Ga have recently been reported in the study area (Shen et al., 2004, 2007; Hou et al., 2008; Wan et al., 2012b, c).

The potassic high Ba–Sr granites for this study were collected from the Wanghailou (08YS-104-118; Fig. 2a) and Hujiazhuang (08YS-104-118; Fig. 2a) granitic intrusions in the Feixian area, and the Xiajiazhuang intrusion in the Zoucheng area (08YS-139-142; Fig. 2b). Their regional distribution is shown in Fig. 1b. All the plutons intrude into late Archean gneisses with ages of ~2.55 Ga (Fig. 2a and b). All samples are biotite monzogranite in composition, although some from the Wanghailou intrusion lie close to the granodiorite field (Fig. 3). All rocks are gray in color, medium- to coarse-grained, and composed of K-feldspar (~25–30%), plagioclase (~27–40%), quartz (~15–25%), and biotite (~10–15%), with minor amounts of zircon, apatite, titanite and Fe oxides. One representative sample from each of these intrusions was selected for zircon U–Pb dating. Sample 08YS-112 was collected from north of Wanghailou Mountain (35°28.665′N, 118°03.304′E; Fig. 2a); sample 08YS-105 was collected from approximately 1 km south of Hujiazhuang village (35°27.488′N, 118°05.875′E; Fig. 2a); and sample 08YS-142 was obtained from near Xiajiazhuang village (35°21.708′N, 117°26.797′E; Fig. 2b).

3. Analytical techniques

3.1. Zircon U–Pb dating

Zircons for LA-ICP-MS dating were separated using conventional heavy liquid and magnetic techniques and then handpicking under a binocular microscope. The zircon grains were mounted in epoxy resin, polished to half their thickness, and then photographed in transmitted and reflected light. The internal structure of the zircons was examined using cathodoluminescence (CL) imaging prior to U–Pb isotopic analysis. The CL images were obtained using an EMPA-JXA-8100 scanning electron microscope at the Guangzhou Institute of Geochemistry, Chinese Academy of Sciences, Guangzhou.

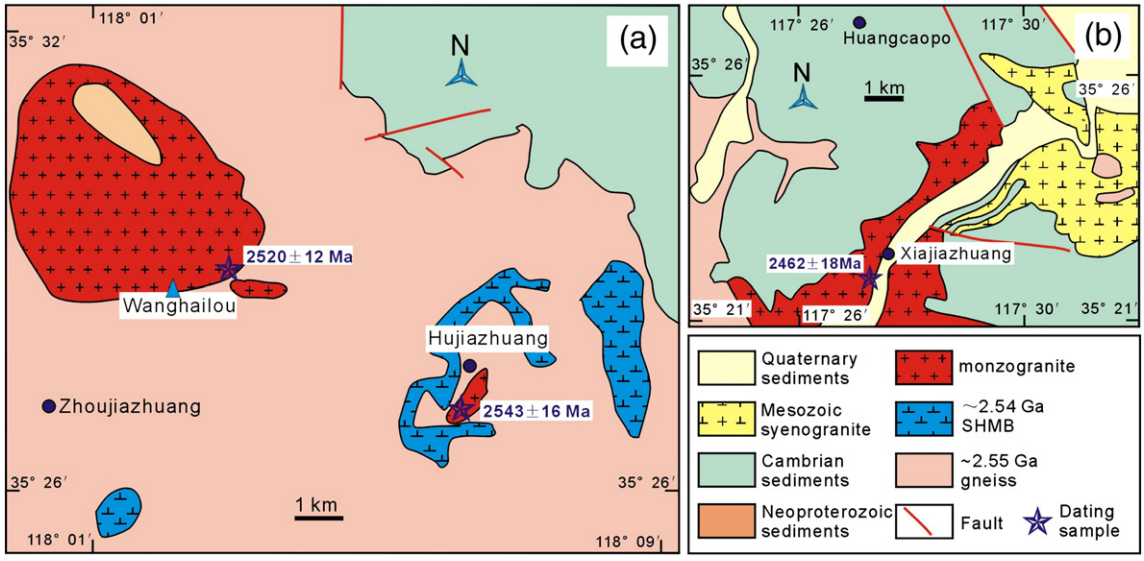

Fig. 2. Geological maps showing the location of the late Neoarchean high Ba–Sr granites. (a) The Wanghailou and Hujiazhuang intrusions and, (b) the Xiajiazhuang intrusion. SHMB = siliceous high-Mg basalt.

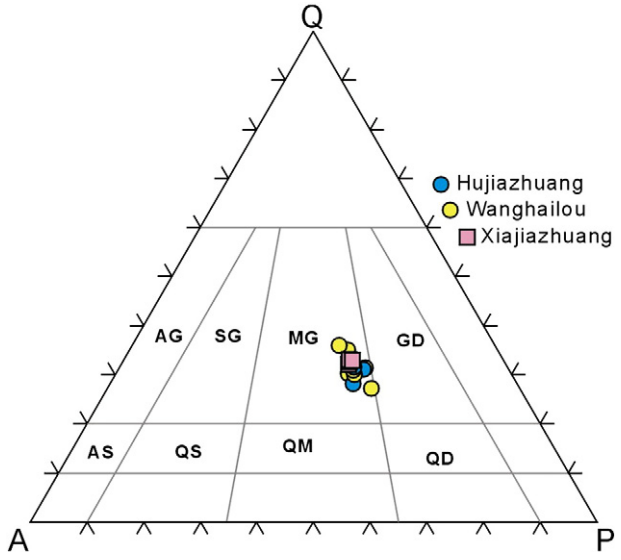

Fig. 3. Classification of the late Neoarchean high Ba–Sr granites from the TSGT according to their modal mineral contents using the QAP diagram (based on Streckeisen, 1976). Q = quartz; A = alkali feldspar; P = plagioclase; AG = alkali-feldspar granite; AS = alkali-feldspar syenite; SG = syenogranite; QS = quartz syenite; MG = monzogranite; QM = quartz monzonite; GD = granodiorite; QD = quartz monzodiorite.

LA-ICP-MS U–Pb dating of zircons was conducted at the State Key Laboratory of Ore Deposit Geochemistry, Institute of Geochemistry, Chinese Academy of Sciences, Guiyang, China. A GeoLasPro laser-ablation system (Lamda Physik, Gottingen, Germany) and Agilent 7700x ICP-MS (Agilent Technologies, Tokyo, Japan) were combined for the experiments. The 193 nm ArF excimer laser, homogenized by a set of beam delivery systems, was focused on the zircon surface with a fluence of 10 J/cm^2. Ablation protocol employed a spot diameter of 32 μm at 5 Hz repetition rate for 40 s (equating to 200 pulses). Helium was the carrier gas used to transport the aerosol to the MS. Zircon 91500 was used as the external standard to correct elemental fractionation, while zircons GJ-1 and Plešovice were also used for quality control. Lead concentration in zircon was externally calibrated against NIST SRM 610 with Si as the internal standard, and Zr as the internal standard for other trace elements (Hu et al., 2011). Data reduction was performed off-line by ICPMS DataCal (Liu et al., 2010a,b). ^{202}Hg is usually <10 cps in the gas blank, therefore the contribution of ^{204}Hg to ^{204}Pb is negligible and is not considered further. Common Pb was corrected according to the method proposed by Anderson (2002). The U–Pb ages were calculated using the U decay constants of Steiger and Jäger (1977) and Isoplot Ex 3 software (Ludwig, 2003). Individual analyses are presented with 1σ error in Table 1, and age uncertainties for pooled data are quoted at the 95% confidence level. U–Pb zircon concordia plots and representative zircon CL images are shown in Fig. 4.

3.2. Zircon Hf isotope analysis

All Hf isotopic compositions of single zircons were determined at the Department of Earth Sciences, the University of Hong Kong. The detailed analytical procedure follows that reported by Xia et al. (2011). Zircon 91500 was used as the external standard with a recommended ^{176}Hf/^{177}Hf ratio of 0.282306 ± 10 (Woodhead et al., 2004). Correction for isobaric interference of ^{176}Lu on ^{176}Hf and ^{176}Yb on ^{176}Hf was performed by using the recommended ^{176}Lu/^{175}Lu ratio of 0.02669 (De and Taylor, 1993) and ^{176}Yb/^{172}Yb ratio of 0.5886 (Chu et al., 2002), respectively. A decay constant for ^{176}Lu of 1.865 × 10^{-11} year^{-1} (Scherer et al., 2001) was adopted in this work. $\varepsilon_{Hf}(t)$ values were calculated using the measured U–Pb ages and with reference to the chondritic reservoir (CHUR) present-day ^{176}Hf/^{177}Hf = 0.282772 and ^{176}Lu/^{177}Hf = 0.0332 (Blichert-Toft and Albarede, 1997). Single-stage Hf model ages (T_{DM1}(Hf)) were calculated relative to the depleted mantle present-day value of ^{176}Hf/^{177}Hf = 0.28325 and ^{176}Lu/^{177}Hf = 0.0384 (Nowell et al., 1998; Vervoort and Blichert-Toft, 1999; Griffin et al., 2000). We also calculated a 'crustal' model age (T_{DM2}(Hf)), which assumes that the parental magma was produced from average continental crust (^{176}Lu/^{177}Hf = 0.015) that originally was derived from the depleted mantle. The zircon Hf analyses were obtained using the same mounts as those used for U–Pb dating and data were collected over the U–Pb spots in most cases but, where this was not possible, they were run on adjacent sites within the same CL domain. The analytical results are listed in Table 2.

3.3. Major and trace element analyses

Major oxide contents were determined at the Guangzhou Institute of Geochemistry, Chinese Academy of Sciences (CAS), Guangzhou, using a wavelength dispersive X-ray fluorescence (XRF) spectrometer with analytical errors better than 2%. Trace element analyses were performed at the Institute of Geochemistry, CAS, Guiyang, China, using an inductively coupled plasma mass spectrometer (ICP-MS). The detailed analytical procedure is described in Qi et al. (2000). The analytical precision is better than 5% for elements >10 ppm, better than 8% for those <10 ppm, and about 10% for transition metals. The analytical results are listed in Table 3.

3.4. Whole-rock Nd isotope analyses

Nd isotopic ratios were measured using a VG 354 mass-spectrometer at the Guangzhou Institute of Geochemistry, CAS, Guangzhou. The mass fractionation corrections for Nd isotopic ratios were normalized to ^{146}Nd/^{144}Nd = 0.7219. Standard La Jolla gave ^{143}Nd/^{144}Nd = 0.511862 ± 10 (n = 6) during the course of the experiments. The whole procedure blanks were less than 50 pg for Nd. The ^{147}Sm/^{144}Nd ratios were calculated using the Sm and Nd contents measured by ICP-MS. The Nd isotopic results are presented in Table 4.

4. Results

4.1. Zircon U–Pb and Lu–Hf results

4.1.1. Wanghailou intrusion

All zircon crystals from sample 08YS-112 are euhedral, equant to elongate in habit (length/width ratio of 2:1), and brown to pink in color. Concentric oscillatory zoning (Fig. 4a), coupled with high Th/U ratios (0.32–1.10; Table 1), indicates a magmatic origin. Of the 21 zircons analyzed, 18 are discordant and 20 zircons define an upper intercept age of 2543 ± 16 Ma; only two zircons plot close to the concordia, giving ^{207}Pb/^{206}Pb ages of 2526 ± 38 Ma and 2520 ± 35 Ma (Fig. 4a). Thus, the age of 2543 ± 16 Ma can be interpreted as the emplacement time of the monzogranite. One analysis falls on concordia and gives an older age of 2633 ± 35 Ma, indicating it is an inherited zircon.

Fifteen zircon grains from the sample were analyzed for Lu–Hf isotopic composition (Table 2). Fourteen analyses of 2520 Ma zircons yielded a relatively low ^{176}Hf/^{177}Hf ratio between 0.281170 and 0.281418 and a wide range of $\varepsilon_{Hf}(t)$ values from −1.06 to +5.67 (Table 2; Fig. 5) with T_{DM2}(Hf) model ages ranging from 2.68 Ga to 3.10 Ga. The older zircon xenocryst yielded an $\varepsilon_{Hf}(t)$ value of +1.61 and T_{DM2}(Hf) model age of 3.00 Ga.

4.1.2. Hujiazhuang intrusion

Zircon grains from sample 08YS-105 have similar morphologies, being mostly transparent, euhedral and light brown in color, with length/width ratios of 2:1 to 4:1. Cathodoluminescence (CL) images indicate that these zircons commonly have concentric oscillatory zoning (Fig. 4b), although some are darker and more homogeneous.

Table 1
LA-ICP-MS U–Pb data for zircons from the potassic high Ba–Sr granites in the Taishan granite–greenstone terrane.

Analysis	Content (ppm)			Th/U	Corrected isotope ratios						Isotope ages (Ma)					
	Th	U	Pb[a]		$^{207}Pb^{a}/^{206}Pb^{a}$	±1σ	$^{207}Pb^{a}/^{235}U$	±1σ	$^{206}Pb^{a}/^{238}U$	±1σ	$^{207}Pb^{a}/^{206}Pb^{a}$	±1σ	$^{207}Pb^{a}/^{235}U$	±1σ	$^{206}Pb^{a}/^{238}U$	±1σ
08YS-112																
YS112-01	140	215	107	0.65	0.1673	0.0028	8.71	0.14	0.3757	0.0041	2531	28	2308	15	2056	19
YS112-02	276	634	220	0.44	0.1639	0.0025	6.59	0.12	0.2886	0.0038	2498	25	2058	16	1634	19
YS112-03	522	1160	231	0.45	0.1688	0.0036	3.45	0.12	0.1470	0.0058	2546	35	1517	27	884	33
YS112-04	114	295	179	0.39	0.1767	0.0035	12.53	0.25	0.5095	0.0065	2633	32	2645	19	2654	28
YS112-05	454	874	189	0.52	0.1586	0.0028	3.69	0.07	0.1678	0.0015	2440	31	1569	14	1000	8
YS112-06	152	176	114	0.87	0.1668	0.0037	11.34	0.27	0.4890	0.0068	2526	38	2551	22	2566	30
YS112-07	1213	1269	329	0.96	0.1661	0.0035	4.60	0.12	0.1986	0.0026	2520	35	1749	21	1168	14
YS112-08	799	1703	232	0.47	0.1592	0.0037	2.23	0.06	0.1010	0.0011	2447	40	1192	17	620	6
YS112-09	828	543	257	1.53	0.1653	0.0058	7.67	0.28	0.3336	0.0102	2511	59	2193	33	1856	50
YS112-10	289	289	189	1.00	0.1651	0.0062	10.95	0.39	0.4768	0.0090	2509	64	2519	33	2513	39
YS112-11	788	843	202	0.93	0.1608	0.0033	4.12	0.09	0.1834	0.0024	2465	33	1657	18	1086	13
YS112-12	735	554	178	1.33	0.1612	0.0041	5.01	0.10	0.2225	0.0042	2468	44	1821	16	1295	22
YS112-13	888	1099	245	0.81	0.1596	0.0028	3.77	0.08	0.1684	0.0031	2452	30	1585	18	1003	17
YS112-14	258	361	165	0.71	0.1664	0.0026	8.09	0.13	0.3469	0.0046	2521	26	2241	14	1920	22
YS112-15	186	280	139	0.66	0.1669	0.0023	9.55	0.15	0.4098	0.0058	2527	22	2393	14	2214	27
YS112-16	291	616	191	0.47	0.1611	0.0024	5.44	0.08	0.2417	0.0029	2478	25	1891	12	1395	15
YS112-17	207	228	103	0.91	0.1705	0.0026	8.07	0.13	0.3386	0.0034	2563	26	2239	14	1880	16
YS112-18	158	283	136	0.56	0.1677	0.0030	8.43	0.15	0.3598	0.0045	2535	29	2278	16	1981	21
YS112-19	511	677	212	0.76	0.1599	0.0024	5.15	0.08	0.2312	0.0020	2455	26	1844	14	1341	10
YS112-20	907	1121	128	0.81	0.1673	0.0055	1.85	0.07	0.0802	0.0030	2531	56	1063	24	497	18
YS112-21	458	968	239	0.47	0.1591	0.0052	4.06	0.14	0.1833	0.0029	2446	54	1646	28	1085	16
08YS-105																
YS105-01	514	832	422	0.62	0.1644	0.0032	8.70	0.17	0.3810	0.0040	2502	33	2307	18	2081	19
YS105-02	577	890	157	0.65	0.1493	0.0025	2.73	0.04	0.1320	0.0013	2339	28	1337	12	799	8
YS105-03	111	257	98	0.43	0.1681	0.0032	6.57	0.14	0.2816	0.0045	2539	33	2055	19	1600	23
YS105-04	119	384	127	0.31	0.1632	0.0024	5.75	0.09	0.2542	0.0027	2500	24	1939	13	1460	14
YS105-05	242	322	165	0.75	0.1640	0.0028	8.52	0.14	0.3740	0.0040	2498	25	2288	15	2048	19
YS105-06	363	479	149	0.76	0.1634	0.0027	5.13	0.07	0.2270	0.0032	2491	28	1840	12	1319	17
YS105-07	125	241	65	0.52	0.1615	0.0022	4.75	0.10	0.2122	0.0037	2472	23	1776	17	1241	20
YS105-08	248	467	132	0.53	0.1616	0.0021	4.94	0.07	0.2195	0.0018	2473	23	1809	11	1279	9
YS105-09	652	789	199	0.83	0.1584	0.0022	4.14	0.05	0.1879	0.0018	2439	23	1663	10	1110	10
YS105-10	1371	2258	192	0.61	0.1554	0.0026	1.40	0.02	0.0646	0.0008	2406	29	888	9	404	5
YS105-11	219	467	172	0.47	0.1648	0.0023	6.76	0.11	0.2946	0.0035	2505	22	2081	14	1664	18
YS105-12	456	793	178	0.58	0.1617	0.0018	3.81	0.05	0.1691	0.0013	2473	19	1595	10	1007	7
YS105-13	439	531	127	0.83	0.1597	0.0018	4.06	0.05	0.1826	0.0012	2454	19	1646	9	1081	6
YS105-14	100	134	64	0.75	0.1623	0.0028	8.29	0.15	0.3669	0.0040	2480	29	2263	17	2015	19
YS105-15	430	631	113	0.68	0.1600	0.0024	3.12	0.05	0.1401	0.0017	2457	25	1437	13	845	10
YS105-16	124	272	115	0.46	0.1612	0.0032	7.63	0.15	0.3393	0.0044	2468	33	2188	18	1883	21
YS105-17	656	951	204	0.69	0.1615	0.0025	3.63	0.06	0.1614	0.0017	2472	21	1557	12	965	9
YS105-18	475	505	274	0.94	0.1635	0.0024	9.55	0.14	0.4185	0.0036	2492	25	2392	13	2254	17
YS105-19	256	550	150	0.47	0.1647	0.0036	4.59	0.08	0.2002	0.0029	2505	38	1747	15	1176	15
YS105-20	501	870	229	0.58	0.1620	0.0038	4.19	0.10	0.1852	0.0031	2477	40	1671	20	1095	17
YS105-21	408	673	213	0.61	0.1610	0.0027	5.59	0.10	0.2492	0.0035	2466	28	1915	15	1434	18
YS105-22	156	167	103	0.94	0.1659	0.0020	10.93	0.15	0.4739	0.0049	2517	21	2517	12	2501	21
YS105-23	1035	1425	217	0.73	0.2265	0.0670	2.44	0.10	0.1089	0.0047	3027	493	1254	30	666	27
08YS-142																
YS142-01	975	955	187	1.02	0.1540	0.0029	2.92	0.05	0.1365	0.0015	2391	37	1387	14	825	9
YS142-02	70	121	75	0.58	0.1607	0.0041	10.47	0.27	0.4682	0.0066	2465	43	2477	24	2476	29
YS142-03	167	167	113	1.00	0.1610	0.0033	10.51	0.22	0.4692	0.0061	2466	34	2481	19	2480	27
YS142-04	185	260	135	0.71	0.1576	0.0026	8.45	0.15	0.3860	0.0041	2431	27	2281	16	2104	19
YS142-05	113	138	90	0.82	0.1613	0.0027	10.58	0.18	0.4721	0.0040	2469	28	2487	16	2493	17
YS142-06	451	569	262	0.79	0.1574	0.0029	7.33	0.15	0.3335	0.0033	2428	33	2152	18	1855	16
YS142-07	77	85	55	0.90	0.1610	0.0029	10.41	0.19	0.4656	0.0043	2466	31	2472	17	2464	19
YS142-08	216	319	197	0.68	0.1610	0.0030	10.47	0.18	0.4683	0.0053	2466	32	2478	16	2476	23
YS142-09	705	759	260	0.93	0.1560	0.0025	5.52	0.09	0.2539	0.0019	2413	26	1904	13	1458	10
YS142-10	97	95	62	1.02	0.1590	0.0027	10.30	0.18	0.4653	0.0038	2456	28	2462	16	2463	17
YS142-11	73	109	67	0.67	0.1607	0.0028	10.45	0.18	0.4682	0.0036	2465	28	2476	16	2475	16
YS142-12	66	84	52	0.79	0.1603	0.0032	10.39	0.20	0.4672	0.0042	2458	33	2471	18	2471	19
YS142-13	203	357	187	0.57	0.1585	0.0030	9.08	0.17	0.4112	0.0031	2439	33	2346	17	2220	14
YS142-14	454	487	237	0.93	0.1556	0.0031	7.50	0.14	0.3460	0.0023	2409	33	2173	17	1916	11
YS142-15	484	638	236	0.76	0.1530	0.0033	6.01	0.13	0.2818	0.0026	2379	37	1977	19	1600	13
YS142-16	765	790	221	0.97	0.1515	0.0031	4.37	0.09	0.2071	0.0017	2365	35	1707	16	1213	9
YS142-17	182	191	123	0.95	0.1607	0.0032	10.49	0.20	0.4688	0.0046	2463	33	2479	18	2478	20
YS142-18	176	250	133	0.70	0.1594	0.0026	9.00	0.13	0.4064	0.0026	2450	27	2338	13	2199	12
YS142-19	552	627	187	0.88	0.1593	0.0024	5.03	0.07	0.2270	0.0018	2448	20	1825	12	1319	9
YS142-20	257	395	216	0.65	0.1611	0.0018	9.43	0.10	0.4198	0.0025	2478	20	2381	10	2260	11
YS142-21	102	99	65	1.03	0.1606	0.0030	10.48	0.20	0.4681	0.0049	2462	31	2479	18	2475	21
YS142-22	137	217	132	0.63	0.1605	0.0032	10.35	0.18	0.4630	0.0066	2461	33	2467	16	2453	29

[a] Radiogenic lead.

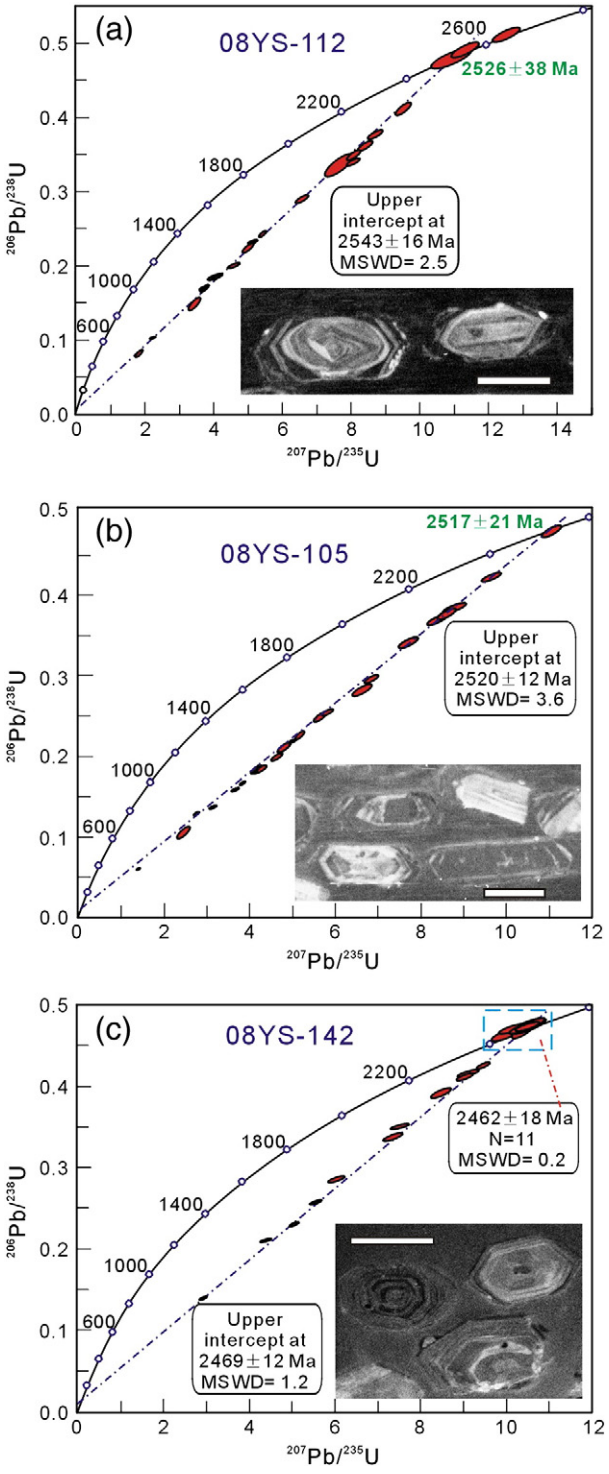

Fig. 4. LA-ICP-MS zircon U–Pb concordia diagrams for the late Neoarchean high Ba–Sr granites in the TSGT of the Eastern Block, North China Craton: (a) 08YS-105, (b) 08YS-112 and (c) 08YS-142. Insets show CL images of typical zircons analyzed. The scale bar is 100 μm long.

Twenty three analyses indicate that the zircons have a relatively wide range in U (134–2258 ppm) and Th (111–1371 ppm) concentrations, with Th/U ratios of 0.31–0.94 (Table 1), similar to those of typical magmatic zircons. The analyses are mostly discordant and define an upper intercept age of 2520 ± 12 Ma (Fig. 4b); only one zircon plots close to concordia and records a $^{207}Pb/^{206}Pb$ age of 2517 ± 21 Ma (Fig. 4b). These results indicate an emplacement age of ~2520 Ma for the Hujiazhuang monzogranite.

Fourteen zircon grains were analyzed for Lu–Hf isotopic composition (Table 2). All analyses yielded a similar range of $^{176}Hf/^{177}Hf$ ratio (0.281130–0.281417) and $\varepsilon_{Hf}(t)$ values (0.88–+6.21) to the Wanghailou granite, barring one analysis (YS-105-3) having a low $\varepsilon_{Hf}(t)$ value (−4.74). Taking into account that the larger error in $^{176}Hf/^{177}Hf$ ratio and lower $\varepsilon_{Hf}(t)$ value for this analysis than the others (Table 2), it is not included in the following discussion. The $T_{DM2}(Hf)$ model ages range from 2.64 Ga to 2.96 Ga (Table 2; Fig. 5).

4.1.3. Xiajiazhuang intrusion

All zircons from sample 08YS-142 are 50–150 μm in size, with length/width ratios of 1:1–3:1. They are euhedral and light brown in color and show magmatic oscillatory zoning in CL (Fig. 4c). The Th and U contents vary from 66 to 975 ppm and 84 to 955 ppm, respectively, with Th/U ratios of 0.57–1.18, also consistent with a magmatic origin. Taken together, all 22 zircons analyzed record an upper intercept age of 2469 ± 12 Ma. Of these, 11 spots are concordant and record a weighted mean $^{207}Pb/^{206}Pb$ age of 2462 ± 18 Ma (Fig. 4c), indicating a crystallization age of ~2460 Ma for the Xiajiazhuang monzogranite.

By comparison with the Wanghailou and Hujiazhuang granites, sample 08YS-142 from the Xiajiazhuang intrusion shows less variation in the $^{176}Hf/^{177}Hf$ ratio from 0.281203 to 0.281277, corresponding to $\varepsilon_{Hf}(t)$ values ranging from −1.00 to +1.96 and $T_{DM2}(Hf)$ model ages of 2.86–3.04 Ga (Table 2; Fig. 5).

4.2. Major and trace element compositions

For comparative purposes when discussing the new data, we have also included on the figures published data for the late Archean mantle-derived sanukitoids (Wang et al., 2009), siliceous high-Mg basalts (SHMBs; Peng et al., 2013), and slab-derived adakitic rocks (Peng et al., 2012) from the TSGT.

All granite samples from the Feixian and Zoucheng areas in the TSTG have relatively constant SiO_2 contents of between 71.91 wt.% and 75.53 wt.%, and low contents of MgO, CaO, Fe_2O_3, TiO_2, P_2O_5, Cr and Ni; their Mg numbers vary from 35 to 44. They are rich in total alkalis ($Na_2O + K_2O$ = 7.91–8.67 wt.%), have high K_2O/Na_2O ratios and plot in the high-potassium calc-alkaline field on the K_2O versus SiO_2 diagram (Peccerillo and Taylor, 1976), revealing an overall potassic character (Fig. 6a). The A/CNK values vary from 1.01 to 1.08, indicating that they are peraluminous (Fig. 6b). On the major element Harker diagrams (Fig. 7a–h), the MgO, Fe_2O_3, Al_2O_3, CaO, P_2O_5, TiO_2 and Na_2O contents decrease with increasing SiO_2 contents, whereas there is no correlation between K_2O and SiO_2. All samples have high Ba contents (up to 2000 ppm) and Sr contents of 198 ppm to 321 ppm (Table 3).

On chondrite-normalized REE diagrams (Fig. 8a–c), all the granites display strongly fractionated REE patterns [$(La/Yb)_{cn}$ = 20.2–57.8 and $(Gd/Yb)_{cn}$ = 1.27–3.26] with weak negative to positive Eu anomalies (δEu = 0.75–1.73) [where 'CN' indicates normalization to chondrite values]. Primordial mantle normalized incompatible trace element patterns (Fig. 8b and d) for all samples are characterized by negative Nb, Ta, P, and Ti anomalies. In addition, marked negative U anomalies in the Wanghailou and Hujiazhuang granites (Fig. 8b) and a slight Ba trough in the Xiajiazhuang granites (Fig. 8d) are evident.

4.3. Sm–Nd isotope compositions

Two samples from each pluton were selected for Sm–Nd analysis and all granites have a narrow range of $^{147}Sm/^{144}Nd$ (0.0862–0.1058) and $^{143}Nd/^{144}Nd$ (0.510789–0.511159) ratios, corresponding to $\varepsilon_{Nd}(t)$ values ranging from −2.88 to +3.51 (Table 4). The $^{147}Sm/^{144}Nd$ ratios are lower than the average continental crustal value of 0.118 (Jahn and Condie, 1995), indicating significant fractionation between Sm and Nd. Therefore, the two-stage Nd model ages (T_{DM2}) calculated using the

Table 2
Lu–Hf isotopic compositions of zircons from the potassic high Ba–Sr granites in the TSGT.

Analysis	$^{176}Hf/^{177}Hf$	±1σ	$^{176}Lu/^{177}Hf$	$^{176}Yb/^{177}Hf$	$^{207}Pb/^{206}Pb$ age (Ma)	$^{176}Hf/^{177}Hf$ (i)	$\varepsilon_{Hf}(t)$	$T_{DM1}(Hf)$ (Ga)	$T_{DM2}(Hf)$ (Ga)	$f_{Lu/Hf}$
08YS-112										
YS-112-1	0.281247	0.000009	0.000884	0.020601	2540	0.281204	1.51	2.79	2.94	−0.97
YS-112-2	0.281418	0.000013	0.002005	0.042136	2540	0.281322	5.67	2.63	2.68	−0.94
YS-112-3	0.281170	0.000007	0.000793	0.017212	2540	0.281132	−1.06	2.89	3.10	−0.98
YS-112-4	0.281284	0.000011	0.002737	0.069708	2633	0.281146	1.61	2.88	3.00	−0.92
YS-112-5	0.281258	0.000011	0.001155	0.027862	2520	0.281203	1.45	2.79	2.94	−0.97
YS-112-6	0.281321	0.000008	0.001843	0.043039	2520	0.281233	2.50	2.76	2.88	−0.94
YS-112-7	0.281340	0.000012	0.001991	0.045073	2520	0.281244	2.91	2.74	2.85	−0.94
YS-112-8	0.281301	0.000009	0.001930	0.049029	2520	0.281209	1.65	2.79	2.93	−0.94
YS-112-9	0.281315	0.000010	0.001163	0.026899	2520	0.281259	3.47	2.72	2.82	−0.96
YS-112-10	0.281347	0.000011	0.000911	0.020648	2520	0.281304	5.04	2.65	2.72	−0.97
YS-112-11	0.281345	0.000014	0.000905	0.020365	2520	0.281301	4.96	2.66	2.73	−0.97
YS-112-12	0.281445	0.000018	0.005514	0.145197	2520	0.281179	0.56	2.87	3.00	−0.83
YS-112-13	0.281292	0.000014	0.001522	0.033573	2520	0.281219	2.02	2.77	2.91	−0.95
YS-112-14	0.281375	0.000009	0.001378	0.030382	2520	0.281309	5.23	2.65	2.71	−0.96
YS-112-15	0.281361	0.000009	0.003150	0.089210	2520	0.281209	1.66	2.80	2.93	−0.91
08YS-105										
YS-105-1	0.281313	0.000015	0.001277	0.029473	2520	0.281252	2.75	2.73	2.85	−0.96
YS-105-2	0.281331	0.000017	0.000979	0.022148	2520	0.281284	3.89	2.68	2.78	−0.97
YS-105-3	0.281130	0.000024	0.001839	0.046767	2520	0.281041	−4.74	3.02	3.30	−0.94
YS-105-4	0.281310	0.000008	0.001072	0.023582	2520	0.281259	3.00	2.72	2.83	−0.97
YS-105-5	0.281380	0.000009	0.001542	0.037613	2520	0.281306	4.67	2.65	2.73	−0.95
YS-105-6	0.281360	0.000019	0.002936	0.068695	2520	0.281219	1.57	2.78	2.92	−0.91
YS-105-7	0.281343	0.000015	0.001333	0.029965	2520	0.281279	3.71	2.69	2.79	−0.96
YS-105-9	0.281347	0.000016	0.002044	0.047835	2520	0.281248	2.62	2.74	2.86	−0.94
YS-105-10	0.281359	0.000010	0.000834	0.019597	2520	0.281319	5.13	2.63	2.70	−0.97
YS-105-11	0.281390	0.000013	0.001377	0.032084	2520	0.281323	5.30	2.63	2.69	−0.96
YS-105-12	0.281293	0.000015	0.001958	0.046343	2520	0.281199	0.88	2.80	2.96	−0.94
YS-105-13	0.281417	0.000010	0.001408	0.032998	2520	0.281349	6.21	2.59	2.64	−0.96
YS-105-14	0.281322	0.000011	0.001635	0.036089	2520	0.281243	2.46	2.74	2.87	−0.95
YS-105-15	0.281308	0.000011	0.001022	0.023739	2520	0.281258	2.99	2.72	2.83	−0.97
08YS-142										
YS-142-1	0.281211	0.000013	0.000235	0.005404	2470	0.281200	−0.23	2.79	2.99	−0.99
YS-142-2	0.281221	0.000009	0.000327	0.007200	2470	0.281205	−0.06	2.78	2.98	−0.99
YS-142-3	0.281244	0.000018	0.000352	0.008263	2470	0.281227	0.72	2.76	2.93	−0.99
YS-142-4	0.281229	0.000015	0.000437	0.010246	2470	0.281208	0.04	2.78	2.97	−0.99
YS-142-5	0.281241	0.000010	0.000272	0.006321	2470	0.281228	0.77	2.75	2.93	−0.99
YS-142-6	0.281220	0.000013	0.000499	0.011716	2470	0.281197	−0.35	2.80	3.00	−0.98
YS-142-7	0.281203	0.000007	0.000519	0.011548	2470	0.281179	−1.00	2.82	3.04	−0.98
YS-142-8	0.281277	0.000009	0.000320	0.007495	2470	0.281262	1.96	2.71	2.86	−0.99
YS-142-9	0.281246	0.000016	0.000338	0.007836	2470	0.281230	0.84	2.75	2.93	−0.99
YS-142-10	0.281263	0.000010	0.000884	0.021983	2470	0.281222	0.52	2.77	2.95	−0.97
YS-142-11	0.281253	0.000011	0.000401	0.009893	2470	0.281234	0.98	2.75	2.92	−0.99
YS-142-12	0.281208	0.000009	0.000343	0.008082	2470	0.281192	−0.53	2.80	3.01	−0.99
YS-142-13	0.281203	0.000011	0.000333	0.008081	2470	0.281187	−0.71	2.81	3.02	−0.99
YS-142-14	0.281214	0.000014	0.000274	0.005872	2470	0.281201	−0.22	2.79	2.99	−0.99
YS-142-15	0.281226	0.000009	0.000929	0.022285	2470	0.281182	−0.89	2.82	3.03	−0.97

The $^{176}Hf/^{177}Hf$ and $^{176}Lu/^{177}Hf$ ratios of chondrite and depleted mantle at the present day are 0.282772 and 0.0332, and 0.28325 and 0.0384, respectively, Blichert-Toft and Albarede (1997) and Griffin et al. (2000). $\lambda = 1.865 \times 10 - 11\ a^{-1}$, Scherer et al. (2001). $(^{176}Lu/^{177}Hf)_c = 0.015$, t = crystallization age of zircon.
$\varepsilon_{Hf}(t) = 10{,}000 \times \{[(^{176}Hf/^{177}Hf)_S - (^{176}Lu/^{177}Hf)_S \times (e^{\lambda t} - 1)] / [(^{176}Hf/^{177}Hf)_{CHUR,0} - (^{176}Lu/^{177}Hf)_{CHUR} \times (e^{\lambda t} - 1)] - 1\}$; $T_{DM1}(Hf) = 1 / \lambda \times \ln\{1 + [(^{176}Hf/^{177}Hf)_S - (^{176}Hf/^{177}Hf)_{DM}] / [(^{176}Lu/^{177}Hf)_S - (^{176}Lu/^{177}Hf)_{DM}]\}$; $T_{DM2}(Hf) = T_{DM1}(Hf) - (T_{DM1}(Hf) - t)((f_{cc} - f_s) / (f_{cc} - f_{DM}))$, In our calculation, $f_{cc} = -0.55$ and $f_{DM} = 0.157$.

same assumption as Keto and Jacobsen (1987), in the range of 2.56 Ga to 3.13 Ga, are considered to be more reliable than the single-stage model ages (T_{DM1}) of between 2.54 and 3.02 Ga (Table 4).

5. Discussion

5.1. Petrological classification

Tarney and Jones (1994) defined an additional type of granite, named the high Ba–Sr granitoids, based on high Sr (>300 ppm) and Ba (>500 ppm) contents, which is distinct from the low Ba–Sr values that characterize the I-, S- and A-type granites of the Phanerozoic (Chappell and White, 1992). According to the difference in Sr and Ba contents, most granites in this study plot in or near the high Ba–Sr granite field, distinct from low Ba–Sr granite (Fig. 9a), and can be classified as high Ba–Sr granite. Although most samples are lower in Sr, than the original criterion of Tarney and Jones (1994), their high Ba and low Rb concentrations (Table 3) result in different trends from the normal low Ba–Sr type granitoids (Fig. 9a), but are similar to the Scottish Caledonian high Ba–Sr granitoids (Tarney and Jones, 1994). Moreover, on the basis of the classification of El Bouseily and El Sokkary (1975) using a similar trace element association of Sr, Ba and Rb, most granites fall within the anomalous granite field with the exception of two plotting on the boundary between the anomalous granite and normal granite, but nonetheless distinguishable from normal granite (Fig. 9b). Also, their strong fractionated REE patterns, lack of pronounced negative Eu anomalies, marked depletion in Nb, Ta, P and Ti (Fig. 8b and d), together with especially low Y and Yb contents in response to high Sr/Y (29.4–116) and La/Yb (30.0–80.6) ratios, are akin to those typical of high Ba–Sr granites (e.g., Tarney

Table 3
Major (wt.%) and trace (ppm) element compositions for the potassic high Ba–Sr granites in the TSGT.

Locality	Wanghailou					Hujiazhuang				Xiajiazhuang			
Sample	08YS-111	08YS-112	08YS-113	08YS-117	08YS-118	08YS-104	08YS-105	08YS-107	08YS-108	08YS-139	08YS-140	08YS-141	08YS-142
SiO_2	73.17	75.53	73.80	75.12	72.59	74.33	74.11	71.91	73.30	73.96	73.85	73.64	73.80
Al_2O_3	14.63	13.59	14.46	13.64	15.08	13.94	14.35	14.79	14.65	13.80	13.81	13.83	13.79
CaO	1.30	1.03	1.14	1.33	1.41	1.18	1.26	1.75	1.37	1.48	1.51	1.53	1.52
MgO	0.33	0.23	0.26	0.38	0.29	0.30	0.29	0.54	0.32	0.48	0.48	0.49	0.47
Fe_2O_3	1.06	0.69	0.85	0.97	1.06	0.85	0.82	1.79	0.87	1.32	1.35	1.45	1.37
K_2O	4.31	4.44	4.58	4.28	4.20	4.39	4.11	4.32	4.66	4.35	4.33	4.33	4.33
MnO	0.02	0.01	0.02	0.02	0.02	0.03	0.02	0.03	0.02	0.03	0.03	0.03	0.03
Na_2O	4.16	3.60	4.09	3.62	4.51	4.04	4.26	3.76	4.07	3.73	3.74	3.73	3.74
P_2O_5	0.04	0.03	0.03	0.04	0.04	0.04	0.04	0.08	0.04	0.05	0.05	0.06	0.05
TiO_2	0.15	0.11	0.14	0.10	0.14	0.13	0.12	0.26	0.12	0.17	0.18	0.18	0.17
LOI	0.61	0.53	0.42	0.36	0.50	0.55	0.39	0.56	0.37	0.49	0.51	0.57	0.57
Total	99.78	99.79	99.79	99.87	99.84	99.79	99.79	99.79	99.79	99.85	99.85	99.85	99.85
Mg#	38	40	38	44	35	42	42	38	42	42	42	41	41
A/CNK	1.05	1.08	1.05	1.05	1.04	1.03	1.04	1.05	1.03	1.02	1.02	1.02	1.01
Sc	3.07	1.90	4.56	2.95	3.46	4.04	2.84	3.28	3.65	3.83	4.09	4.61	3.85
V	8	6	5	12	10	10	9	15	9	17	17	18	16
Cr	33	36	21	23	13	66	69	41	23	12	17	18	12
Co	30	40	38	41	45	39	31	38	42	36	38	51	50
Ni	14	16	11	15	15	28	29	19	11	7	10	54	8
Ga	13.8	12.7	13.0	15.0	14.3	14.7	15.5	15.8	15.5	13.7	14.1	14.5	14.0
Rb	92.1	100	92.0	98.1	74.4	100	107	140	126	120	118	124	125
Sr	307	286	300	312	267	198	243	321	251	279	284	288	291
Y	4.09	3.08	5.07	2.68	5.56	6.73	5.16	6.87	4.85	5.48	5.59	6.35	6.37
Zr	89	72	102	57	99	73	73	74	84	97	91	98	99
Nb	3.31	1.79	2.68	2.50	2.91	6.58	3.78	6.87	3.69	5.17	4.86	4.76	4.64
Cs	1.14	1.32	1.44	2.55	1.79	2.47	3.24	3.92	2.10	1.93	2.34	2.01	2.02
Ba	1670	1660	1940	1990	901	723	821	1290	856	832	820	820	840
La	23.4	17.5	22.9	9.57	14.9	17.2	14.9	54.9	19.5	23.0	24.4	27.3	27.6
Ce	47	36.7	44.9	19.3	34.7	35.0	30.1	83.9	39.2	44.4	47.7	54.8	55.0
Pr	5.86	4.28	5.43	2.07	3.55	4.38	3.61	8.23	4.96	3.95	4.15	4.63	4.61
Nd	20.4	14.5	19.0	7.54	13.3	15.8	12.9	24.5	17.7	12.9	13.4	14.8	14.9
Sm	3.09	2.18	3.04	1.23	2.32	2.75	2.26	2.82	3.05	1.84	1.99	2.24	2.15
Eu	0.95	0.90	1.00	0.55	0.53	0.60	0.64	0.71	0.63	0.39	0.42	0.44	0.46
Gd	1.58	1.12	1.53	0.62	1.15	1.74	1.41	1.71	1.68	1.02	1.07	1.12	1.10
Tb	0.23	0.17	0.22	0.11	0.22	0.29	0.23	0.26	0.28	0.19	0.21	0.23	0.22
Dy	0.84	0.61	0.94	0.45	0.97	1.23	0.96	1.09	1.02	0.87	0.94	0.99	1.00
Ho	0.15	0.12	0.17	0.09	0.19	0.24	0.18	0.23	0.18	0.18	0.19	0.22	0.21
Er	0.46	0.34	0.55	0.26	0.56	0.64	0.50	0.74	0.50	0.59	0.61	0.62	0.64
Tm	0.06	0.05	0.07	0.03	0.07	0.08	0.07	0.10	0.06	0.08	0.08	0.09	0.10
Yb	0.43	0.33	0.54	0.26	0.53	0.57	0.46	0.68	0.43	0.61	0.60	0.69	0.69
Lu	0.08	0.06	0.10	0.04	0.08	0.09	0.08	0.11	0.06	0.09	0.10	0.11	0.11
Hf	2.40	2.12	2.93	1.59	2.70	2.44	2.39	5.48	2.58	2.89	2.62	2.92	2.87
Ta	0.34	0.30	0.48	0.38	0.42	0.65	0.44	0.80	0.35	0.79	0.84	0.86	0.83
Pb	15.1	17.5	15.3	13.8	13.1	16.1	17.2	19.8	16.4	17.6	17.7	18.4	18.3
Th	11.6	7.07	10.3	2.94	6.65	8.64	6.35	16.2	9.07	13.0	13.2	16.0	14.3
U	1.07	0.64	0.95	0.42	1.01	0.92	0.89	1.36	0.88	2.48	2.36	2.77	2.68

A/CNK = (mol. Al_2O_3/(CaO + K_2O + Na_2O)), Mg# = (100 × molar MgO/(MgO + FeO)), FeO = 0.8998 × Fe_2O_3.

and Jones, 1994; Fowler et al., 2001; Qian et al., 2003; Fowler et al., 2008; Ye et al., 2008; Choi et al., 2009). In this respect, such characteristics are also similar to those of the Archean TTGs (or adakites; Martin et al., 2005), sanukitoids (e.g., Smithies and Champion, 2000; Halla, 2005; Kovalenko et al., 2005; de Oliveira et al., 2009; Martin et al., 2009; de Oliveira et al., 2010), and particularly the potassium-rich Closepet-type granites that were emplaced shortly after sanukitoid magmas (e.g., Moyen et al., 2001, 2003). However, it is evident that the lower Mg number and P_2O_5 contents and higher K_2O/Na_2O ratios of all potassic granites in this study are comparable to typical Phanerozoic high Ba–Sr granites (Fig. 10a–c; Tarney and Jones, 1994; Fowler et al., 2001; Moyen et al., 2001, 2003; Qian et al., 2003; Fowler et al., 2008; Ye et al., 2008; Choi et al., 2009), and are distinct from Archean sanukitoids and the Closepet-type granites (e.g., Smithies and Champion, 2000; Halla, 2005; Kovalenko et al., 2005; de Oliveira et al., 2009; Martin et al., 2009; de Oliveira et al., 2010). They are also distinguishable from the late Archean sanukitoids and adakitic intrusions in the study area (see Fig. 10a–c; Wang et al., 2009; Peng et al., 2012).

5.2. Petrogenesis

The high Ba–Sr granites are geochemically distinct from the traditional I-, S-, and A-type granites and their petrogenesis is still a matter of debate, with different mechanisms proposed to generate their high Ba–Sr contents. For example, Tarney and Jones (1994) proposed that they were probably derived by (1) the partial melting of subducted ocean islands or ocean plateaus, (2) the partial melting of underplated mafic rocks, or (3) the partial melting of veined lithospheric mantle that had been metasomatized by asthenosphere-derived carbonatitic melts; in addition, some authors interpreted them as the products of partial fusion of the mafic lower crust (e.g., Ye et al., 2008; Choi et al., 2009), whereas other workers invoked an origin of enriched subcontinental lithospheric mantle to account for their genesis (e.g., Fowler and Henney, 1996; Fowler et al., 2001; Qian et al., 2003; Fowler et al., 2008). Alternatively, taking into account their similar geochemical signatures to sanukitoids and TTGs, such as high Ba–Sr contents, Sr/Y and $(La/Yb)_{cn}$ ratios and strongly fractionated REE patterns, and close

Table 4
Nd isotopic compositions of selected potassic high Ba–Sr granites in the TSGT.

Sample	Nd	Sm	$^{147}Sm/^{144}Nd$	$^{143}Nd/^{144}Nd$	$\pm 2\sigma$	$\varepsilon_{Nd}(t)$	$f_{Sm/Nd}$	T_{DM1}(Ga)	T_{DM2}(Ga)
08YS-112	14.5	2.18	0.0908	0.510789	4	−1.50	−0.54	2.91	3.02
08YS-113	19.0	3.04	0.0966	0.510816	4	−2.88	−0.51	3.02	3.13
08YS-105	12.9	2.26	0.1058	0.511000	3	−2.52	−0.46	3.02	3.08
08YS-108	17.7	3.05	0.1041	0.511159	4	1.17	−0.47	2.75	2.79
08YS-139	12.9	1.84	0.0862	0.511018	4	3.51	−0.56	2.54	2.56
08YS-142	14.9	2.15	0.0872	0.510952	4	1.91	−0.56	2.63	2.69

Notes: Chondrite uniform reservoir values, $^{147}Sm/^{144}Nd = 0.1967$, $^{143}Nd/^{144}Nd = 0.512638$, are used for the calculation. T_{DM1} values are calculated based on present-day $(^{147}Sm/^{144}Nd)_{DM} = 0.2137$ and $(^{143}Nd/^{144}Nd)_{DM} = 0.51315$. Sm and Nd in ppm. $T_{DM1} = 1/\lambda \times \ln\{1 + [(^{143}Nd/^{144}Nd)_s - 0.51315] / [(^{147}Sm/^{144}Nd)_s - 0.2137]\}$; $T_{DM2} = T_{DM1} - (T_{DM1} - t) \times ((f_{cc} - f_s) / (f_{cc} - f_{DM}))$; Where s = sample. f_{cc}; f_s and f_{DM} are the f_{Sm} = Nd values of the continental crust, the sample and the depleted mantle, respectively. In our calculation, $f_{cc} = -0.4$ and $f_{DM} = 0.08592$; where t = the formation age of the rock.

space–time distribution with the latter, the petrogenesis of high Ba–Sr granites may be related to these rocks or their fractionation products (Smithies et al., 2004; Fowler et al., 2008).

All high Ba–Sr granites in the TSGT are characterized by high SiO_2 and K_2O, and A/CNK and K_2O/Na_2O ratios (most >1), as well as low MgO, Cr and Ni concentrations. These features indicate a crustal source. Nevertheless, the products of partial melting of tholeiitic, calc-alkaline, and alkaline basaltic amphibolites in the lower crust generally have K_2O contents too low to allow evolution into the high-K_2O field (Fig. 6a). An origin from newly formed lower crust can also not account for such signatures. When considering their high Sr/Y and La/Yb ratios, they are comparable to Archean TTG (Watkins et al., 2007). However, the higher SiO_2 contents and higher K_2O/Na_2O, Sr/Y and $(La/Yb)_{cn}$ ratios than Archean TTGs (generally with $K_2O/Na_2O < 0.5$, Martin et al., 2005; Moyen, 2011), imply that typical amphibolite-facies sodic TTGs observed in many Archean terranes could not produce melts with such a potassium-enriched character (Kleinhanns et al., 2003). Moreover, the experimental results of Watkins et al. (2007) corroborated that the potassic high Ba–Sr magmas could not be formed by reworking (partial melting) of sodic-rich TTGs in the lower crust. Indeed, these potassic high Ba–Sr granites in the TSGT have higher Mg numbers and SiO_2 contents and do not plot within the experimental melt field of partial melting of metabasic rock at 1–4 GPa (Fig. 11). This precludes that they were directly derived from partial melting of normal basic lower crust or a subducting oceanic slab (Martin, 1999; Rapp et al., 1999; Condie, 2005). Partial melting of overthickened lower crust with a residue of garnet can account for the highly fractionated REE patterns, very low HREE contents and some positive Eu anomalies in the high Ba–Sr granites (Smithies, 2000). Nonetheless, according to the experimental results of Rapp et al. (2002), based on high-pressure partial melting, it is difficult to explain the potassium-rich character of these granites. In particular, the overthickened crust may not have developed in a volcanic arc (see the discussion in Section 5.4). Additionally, the high Ba–Sr granites in the TSGT possess lower Sr abundances than normal adakitic magma (generally >500 ppm, Martin et al., 2005), also inconsistent with an origin from partial melting of either mafic lower crust or a downgoing oceanic slab; or their fractional crystallization products. The lower Nb/La ratios (0.10–0.38) in the high Ba–Sr granites than the

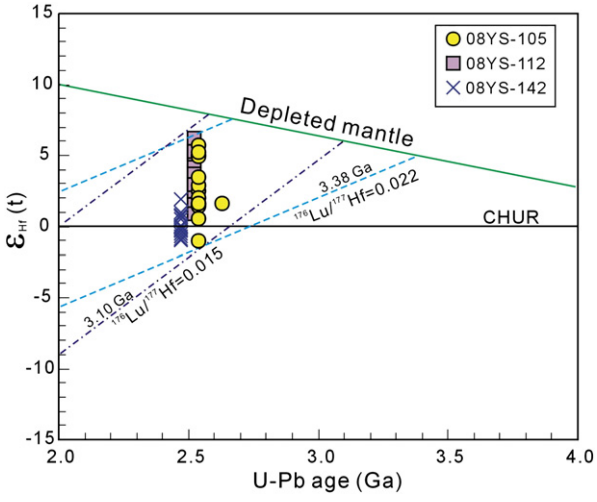

Fig. 5. Plot of zircon $\varepsilon_{Hf}(t)$ versus U–Pb age for the late Neoarchean high Ba–Sr granites in the TSGT. t = crystallization age of zircon. The corresponding lines of crustal extraction are calculated by assuming the $^{176}Lu/^{177}Hf$ ratio of 0.015 for the average continental crust (Griffin et al., 2002) and $^{176}Lu/^{177}Hf$ ratio of 0.022 for the mafic lower crust (Amelin et al., 1999).

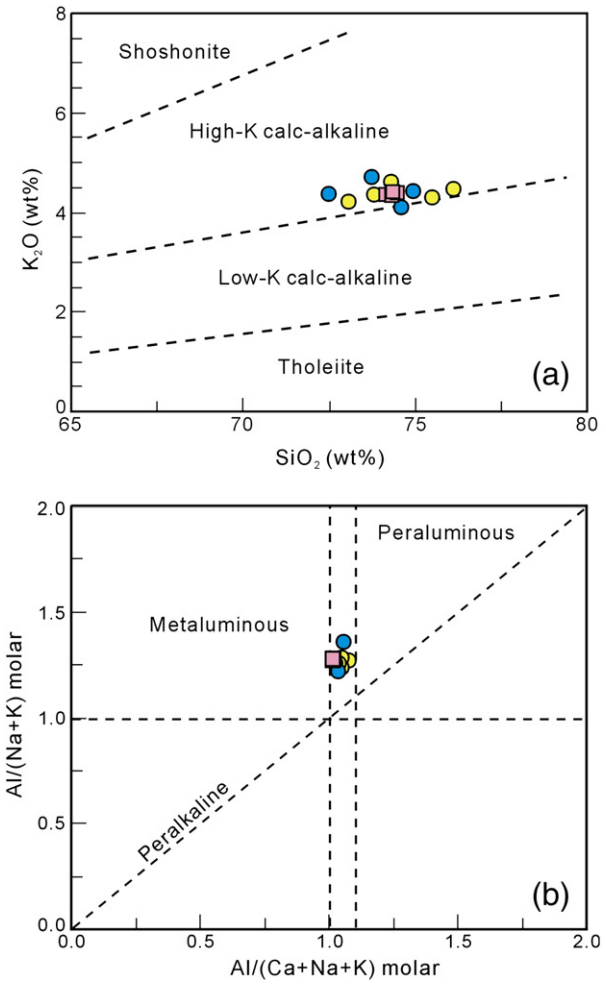

Fig. 6. (a) K_2O versus SiO_2 (after Winchester and Floyd, 1977); (b) molar Al/(K + Na) versus Al/(Ca + Na + K) diagram (after Maniar and Piccoli, 1989) for the high Ba–Sr granites in the TSGT. Symbols are as in Fig. 5.

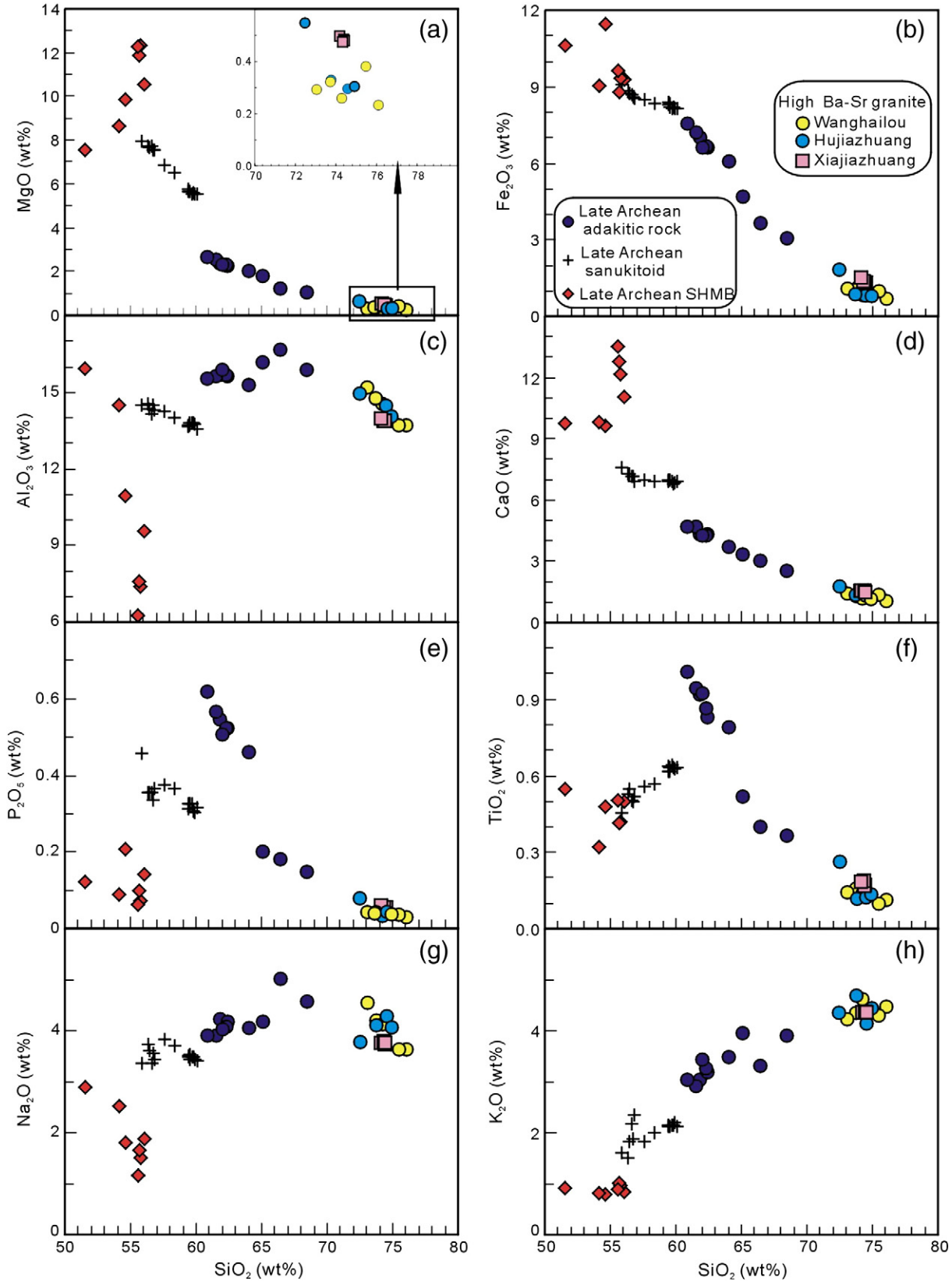

Fig. 7. Harker variation diagrams for the late Neoarchean high Ba–Sr granites in the TSGT. The late Archean sanukitoids, adakitic rocks and SHMB (siliceous high-Mg basalt) are from Wang et al. (2009) and Peng et al. (2012, 2013).

lower continental crust (~0.6; Sun and McDonough, 1989), resemble those of island arc basalts (Hawkesworth and Kemp, 2006b), also inconsistent with an origin from lower continental crust.

Alternatively, due to the higher geothermal gradient in the Archean, a buoyant oceanic plateau would be difficult to subduct beneath the sub-arc mantle (Wyman et al., 2002). In this case, it is impossible that

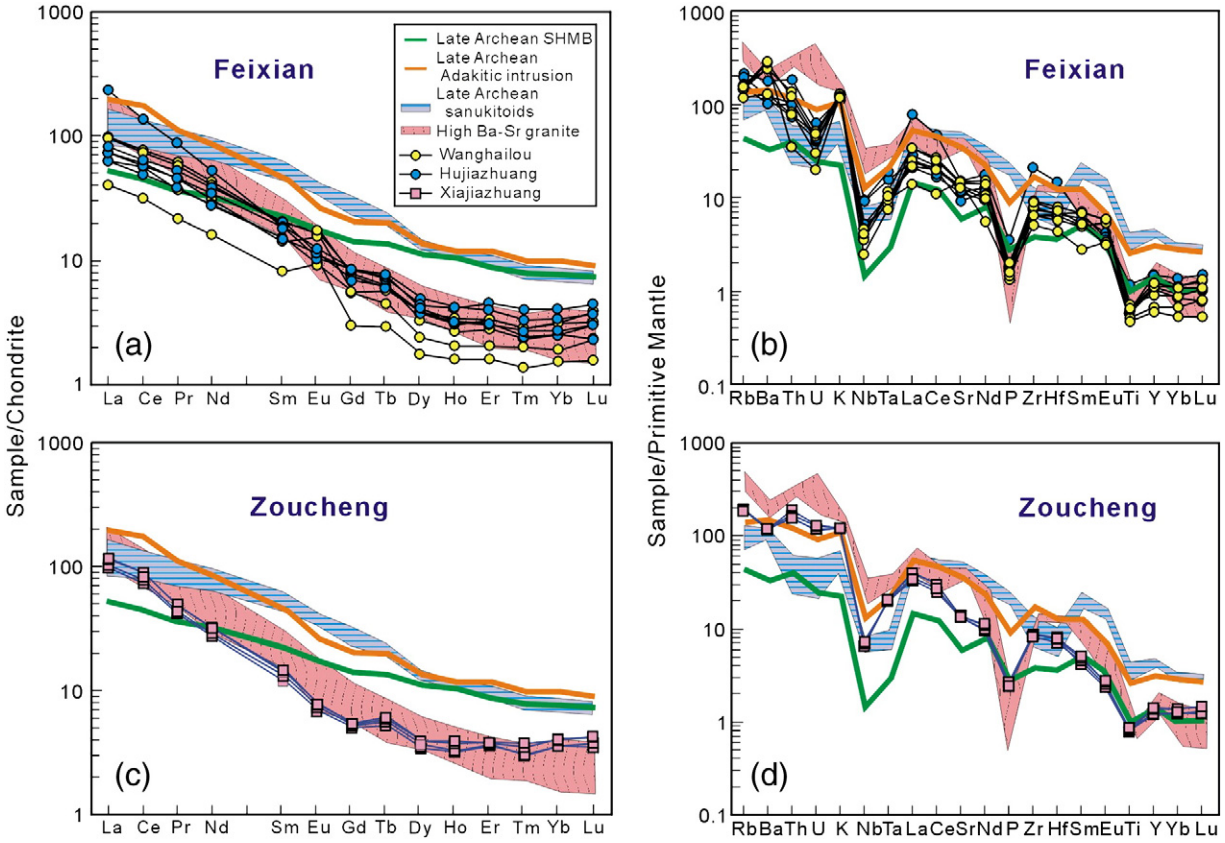

Fig. 8. Chondrite-normalized REE patterns and primitive-mantle-normalized spidergrams for the late Neoarchean high Ba–Sr granites in the TSGT. (a, b) the Feixian area and (c, d) the Zoucheng area. The late Archean sanukitoids are from Wang et al. (2009). The late Archean adakitic intrusions and SHMBs are from Peng et al. (2012, 2013). High Ba–Sr granites are from Fowler et al. (2001, 2008), Qian et al. (2003), Ye et al. (2008), and Choi et al. (2009). Normalizing values of chondrite and primitive mantle are from Taylor and McLennan (1985) and Sun and McDonough (1989), respectively. Symbols are as in Fig. 7.

these potassic high Ba–Sr granites were derived from partial melting of subducted ocean islands or ocean plateaus, as suggested by Tarney and Jones (1994). Consequently, a more feasible mechanism might involve the highly enriched sub-arc mantle (Watkins et al., 2007) to generate these high Ba–Sr granitic magmas in the TSGT. In this regard, the petrogenesis of the high Ba–Sr granites is comparable to those of the late Archean sanukitoids that are characterized by high Ba–Sr, Sr/Y and $(La/Yb)_{cn}$ and highly fractioned REE patterns (Fig. 8a and c) as reported by Wang et al. (2009). Nevertheless, compared with the late Archean sanukitiods (Sr = 608–966 ppm and Ba = 576–635 ppm,

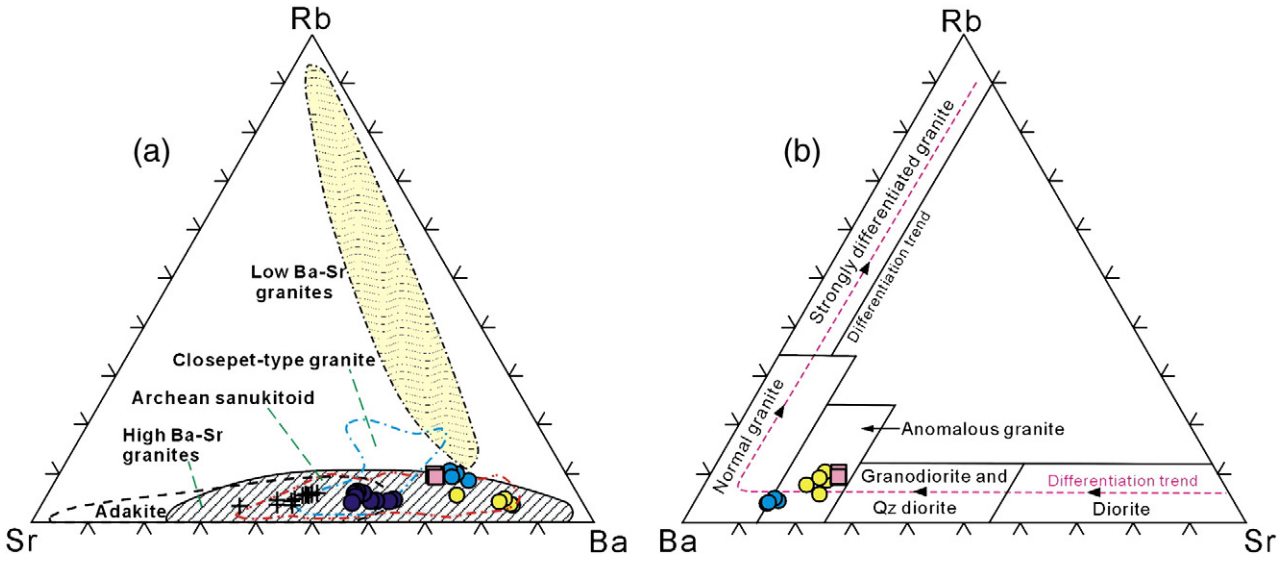

Fig. 9. (a) Sr–Rb–Ba plot (after Tarney and Jones, 1994), and (b) Rb–Ba–Sr plot (after El Bouseily and El Sokkary, 1975) for the late Neoarchean high Ba–Sr granites in the TSGT. Fields of high Ba–Sr and low Ba–Sr granitoids are based on data from Fowler and Henney (1996) and Fowler et al. (2001). Fields of adakite are based on data from Defant et al. (1991a,b), Sajona et al. (1993, 1994), Morris (1995), Stern and Kilian (1996) and Yogodzinski et al. (1994, 1995). Field of Archean sanukitoid is based on data from Stevenson et al. (1999), Smithies and Champion (2000), Halla (2005), Lobach-Zhuchenko et al. (2005, 2008), Larionova et al. (2007), de Oliveira et al. (2009), and Martin et al. (2009). Field of Closepet granite is from Moyen et al. (2001, 2003). Symbols are as in Fig. 7.

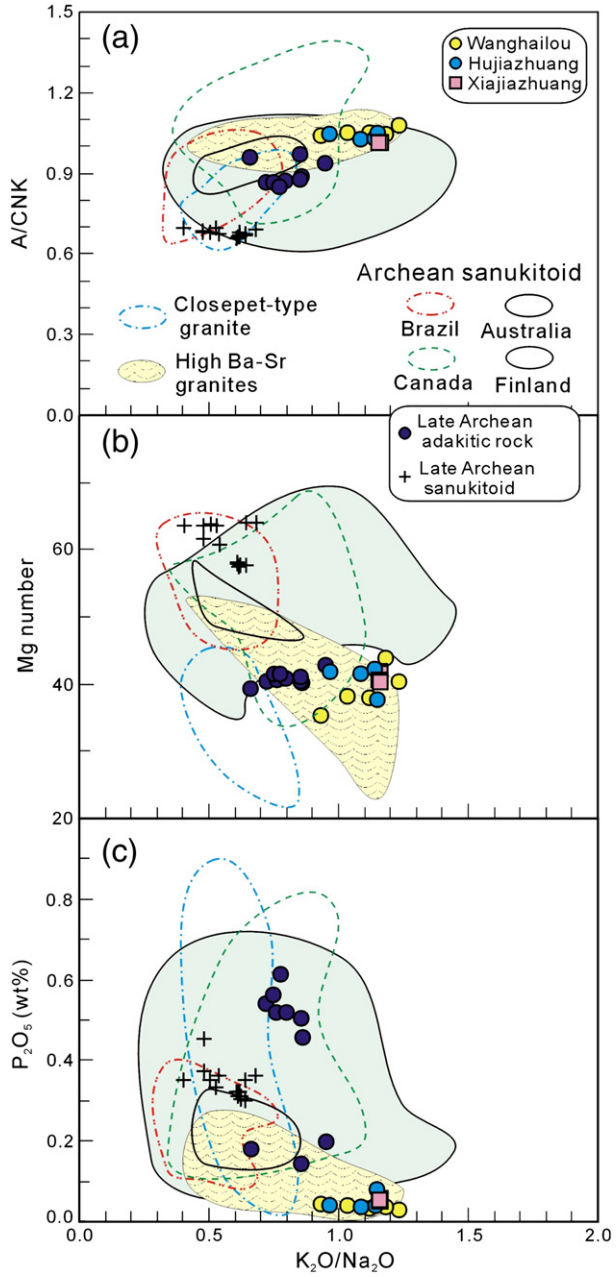

Fig. 10. (a) A/CNK, (b) Mg-number and (c) P_2O_5 versus K_2O/Na_2O plots for the late Neoarchean high Ba–Sr granites in the TSGT. The fields of Archean sanukitoids are from Brazil (de Oliveira et al., 2009), Australia (Smithies et al., 2004), Canada (Stevenson et al., 1999) and Finland (Halla, 2005; Lobach-Zhuchenko et al., 2005). The Closepet-type granite is from Moyen et al. (2001, 2003). High Ba–Sr granites are from Fowler et al. (2001, 2008), Qian et al. (2003), Ye et al. (2008) and Choi et al. (2009).

Wang et al., 2009) in the study area, their lower Sr and higher Ba contents, and slightly lower LREE contents (Fig. 8a and c), along with insignificant fractional crystallization of plagioclase, indicate that pure fractional crystallization of a sanukitoid parental magma could not produce these high Ba–Sr granites. In addition, the Nd isotopic characteristics preclude the possibility of simple mixing between sanukitoid melt ($\varepsilon_{Nd}(t) = +1.53$–$+3.30$) and continental crustal rocks with low Ba–Sr (<300 ppm) contents. Compared with the late Archean siliceous high-Mg basalts (SHMBs) in the study area (Peng et al., 2013), the absence of negative Zr and Hf anomalies in the high Ba–Sr granites (Fig. 8) argues against a simple magmatic differentiation–fractionation model or a two component mixing model for the genesis of high Ba–Sr granites. Furthermore, a distinct compositional gap in SiO_2 and

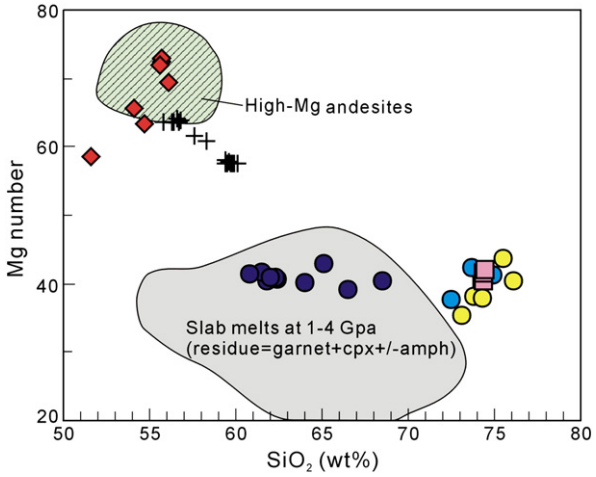

Fig. 11. Mg number versus SiO_2 for the late Neoarchean high Ba–Sr granites in the TSGT. Experimental melt compositions are from Rapp et al. (1999, and references therein). High-Mg andesites are from Yogodzinski et al. (1994) and Shimoda et al. (1998). Symbols are as in Fig. 7.

MgO (Fig. 7) between the high Ba–Sr granites and the SHMB (Peng et al., 2013) does not support a petrogenetic link between them. In Fig. 12a–d, the lack of a linear correlation between the high Ba–Sr granites and the adakitic intrusions, the SHMBs, and the sanukitoids is also inconsistent with an origin from fractional crystallization (AFC) of the latter. Thus, a more viable explanation is that these high Ba–Sr granites originated from a different enriched mantle source.

5.3. Nature of the magma source

The distinct enrichment in LREE and LILE and depletion in HFSE (Nb, P and Ti) in the high Ba–Sr granites may indicate that their mantle source experienced subduction-related fluid or melt metasomatism before partial fusion (e.g., Rapp et al., 1999; Prouteau et al., 2001). Based on the pronounced enrichment in Sr (thousands of ppm) and LREE (La/Yb ca. 10) in carbonatite (Plank and Langmuir, 1998), some authors advocated carbonate metasomatism to explain the genesis of high Ba–Sr granites (Tarney and Jones, 1994; Fowler et al., 2008). However, in comparison with the typical high Ba–Sr granites with Sr contents over 500 ppm (Tarney and Jones, 1994; Fowler et al., 2008), the TSGT potassic rocks possess relatively lower Sr abundances (<400 ppm), but with some having higher Ba contents (up to 2000 ppm; Table 3), and this is inconsistent with an origin related to carbonate metasomatism (LaFlèche et al., 1998). Furthermore, the low-P_2O_5 characteristics of all high Ba–Sr granites are in disagreement with carbonatitic melt metasomatism as described by Green and Wallace (1988), Ionov et al. (1993) and Rudnick et al. (1993). Thus possible melt-related metasomatism from pelagic sediments that commonly have enhanced Ba (thousands of ppm), and are invariably enriched in LREE (La/Yb ca. 10, Plank and Langmuir, 1998) could reasonably explain such enriched features in their mantle source.

However, an alternative mechanism is required to account for the potassium-rich nature of the high Ba–Sr granites. A possibility is that the involvement of terrigeneous sediments in their mantle source, typically having high K_2O/Na_2O (Plank and Langmuir, 1998), could generate the amount of K_2O required. Also, it is well known from studies of arc magmas that fluids released from a subducting slab are hydrous and enriched in alkalis, LILE and LREE, due to the breakdown of hydrous phases in the subducting basaltic crust (Schmidt and Poli, 1998; Scambelluri and Philippot, 2001). This process will create potassium-rich volatile-bearing phases such as phlogopite, K-richterite and pargasite in the mantle source (Canning et al., 1996; Maury et al., 1996; Ionov et al., 1997; Fowler et al., 2001). For

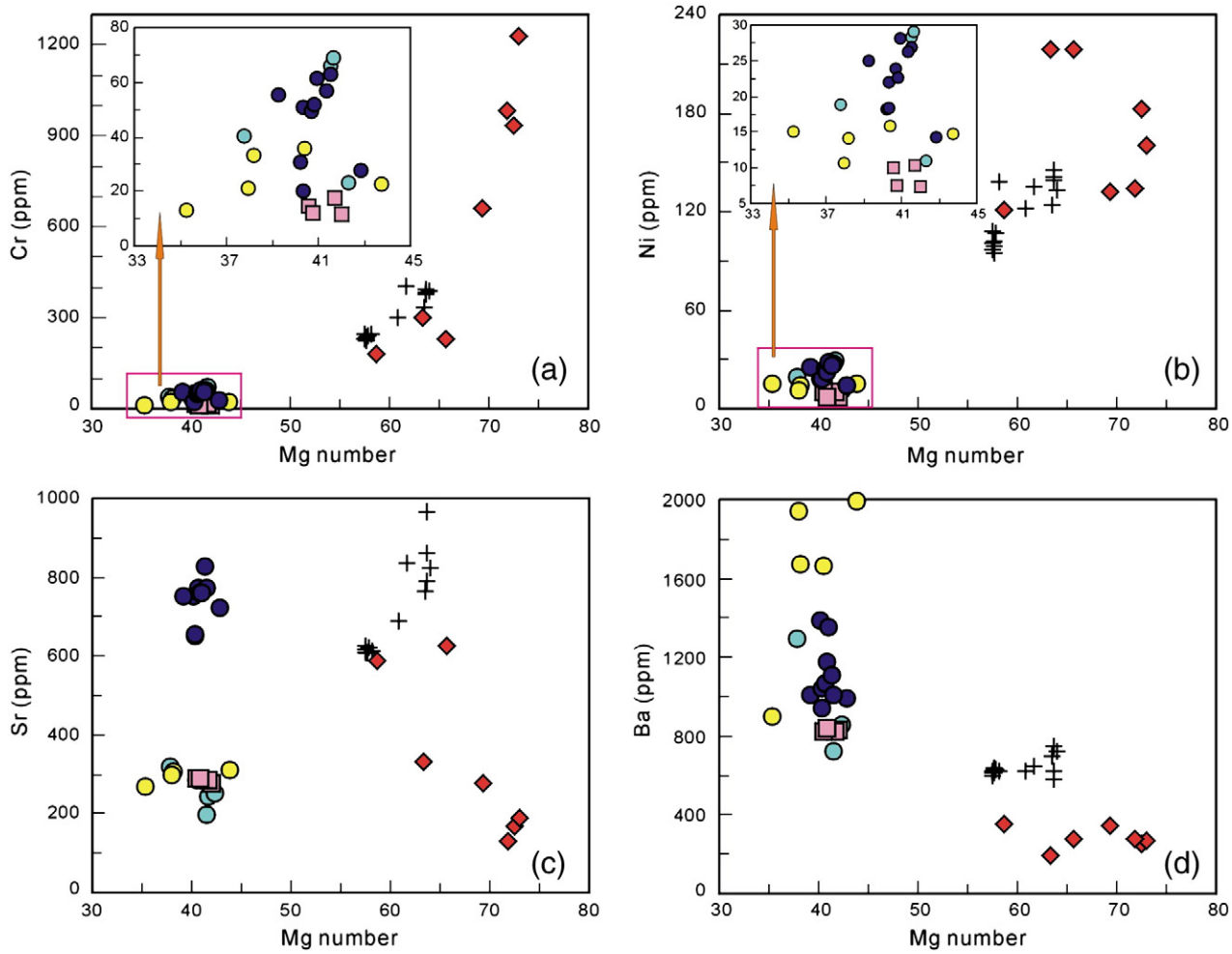

Fig. 12. (a) Cr, (b) Ni, (c) Sr and (d) Ba versus Mg number plots for the late Neoarchean high Ba–Sr granites in the TSGT. Symbols are as in Fig. 7.

the ~2.54 Ga high Ba–Sr granites from the Wanghailou intrusion, a trend of fluid-related enrichment, coupled with a weak trend of melt-related enrichment, is observed in Fig. 13a–c, confirming that the main agents of mantle metasomatism are H_2O-rich fluids, together with a contribution from silicic (adakitic, TTG) melts (Schiano et al., 1995; Kilian and Stern, 2002). In the case of the ~2.52 and ~2.47 Ga high Ba–Sr granites from the Hujiazhuang and Xiajiazhuang intrusions, respectively, an exclusive melt-related enrichment is evident (Fig. 13a–c), indicating involvement of melt generated from partial melting of subducted pelagic and terrigenous sediments. Metasomatism by all the above agents can result in the high LREE and LILE enrichment and marked depletion in Nb and Ti (Weaver, 1991; Aldanmaz et al., 2000). Similarly, this metasomatic process could also be responsible for the anomalously low Rb content in the high Ba–Sr granites, as recognized by El Bouseily and El Sokkary (1975).

Taking into account the strongly fractionated REE, highly enriched LREE and depletion in HREE seen in all high Ba–Sr granites from the TSGT, their parental magma could have originated from partial melting of highly-enriched mantle (previously depleted mantle) at high pressures (>15 kbar) with garnet in the residue. In the Sr/Y versus Y plot (Fig. 14), all high Ba–Sr granites show an evolutionary trend from partial melting of eclogite (Drummond and Defant, 1990), supporting this interpretation. The fractionation of Ti- and P-bearing phases, such as titanite and ilmenite/magnetite, without amphibole, would lead to depletion of Nb, P, and Ti in the PM-diagrams (Fig. 8b and d) and no pronounced negative Eu anomaly, since plagioclase would not be a residual phase. Similarly, plagioclase and alkali-feldspar crystal fractionation must have been insignificant since the rocks contain high K_2O, Na_2O and Ba contents (Table 3). It is also likely that their parental magma was contaminated by older crustal components during magmatic evolution. This process would account for the heterogeneous whole rock $\varepsilon_{Nd}(t)$ (Table 4) and zircon $\varepsilon_{Hf}(t)$ (Table 2). In this regard, the petrogenesis of the high Ba–Sr granites is comparable to those of the late Archean Closepet-type granites (e.g., Jayananda et al., 1995, 2000; Moyen et al., 2001, 2003; Castro, 2004).

5.4. Tectonic environment

The tectonic setting for generating the ~2.7–2.5 Ga greenstones and granitic rocks in the TSGT has been a controversial issue. For example, based on the counterclockwise P–T path of the ~2.5 Ga granulites, together with the occurrence of Late Archean komatiites in the region, Zhao et al. (1998, 2001, 2007) considered that a mantle plume was the most plausible scenario to explain both regional metamorphism and the formation of Late Archean magmatic rocks within the Eastern Block of the North China Craton. Similarly, taking into account the presence of anomalously high-temperature komatiitic rocks (e.g., Polat et al., 2006; Cheng and Kusky, 2007), and the absence of alkali intrusions and adakites with relatively high MgO, Cr, and Ni concentrations in the Late Archean, Yang et al. (2008) also argued that the Neoarchean magmatism and continental crustal development in the Eastern Block of the North China Craton were the result of contemporaneous mantle plume activity. In contrast, a study of the 2.8–2.7 Ga greenstone belt in western Shandong by Polat et al. (2006) invoked a geodynamic model of plume–craton interaction to explain the geological and geochemical characteristics of the Taishan greenstone belt within the TSGT. They

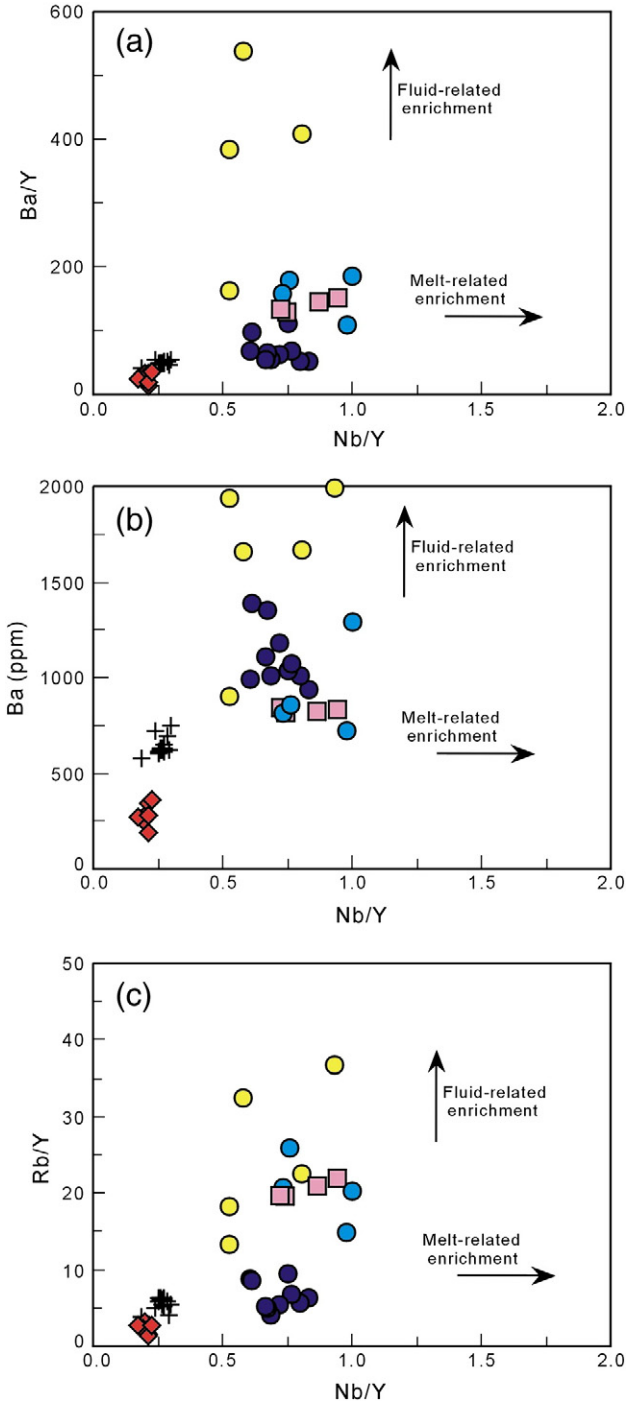

Fig. 13. (a) Ba/Y, (b) Ba and (c) Rb/Y versus Nb/Y plots for the late Neoarchean high Ba–Sr granites in the TSGT. The trends shown in (a–c) are from Kepezhinskas et al. (1997). Symbols are as in Fig. 7.

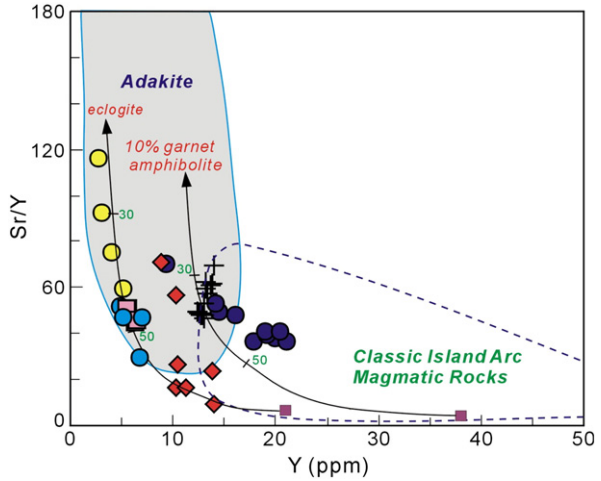

Fig. 14. Sr/Y versus Y plot (after Drummond and Defant, 1990; Martin, 1994) for the late Neoarchean high Ba–Sr granites in the TSGT. Fields of adakites, and classic island arc magmatic rocks are from Defant and Drummond (1990) and Martin et al. (2005). Partial melting curves for basalt leaving residues of eclogite and garnet (10%) amphibolite from Drummond and Defant (1990). Labeled tick marks indicate percent partial melting. Symbols are as in Fig. 7.

also proposed an alternative model of arc–plume interaction to possibly account for the presence of ~2.7 Ga komatiitic rocks and spatially associated late (~2.6 Ga) calc-alkaline andesitic to rhyolitic volcanic rocks in the region (Polat et al., 2006). More recently, a subduction model has been considered responsible for the generation of the ~2.54 Ga igneous rocks on the basis of the identification of sub-arc enriched mantle-derived magma, including sanukitoids (Wang et al., 2009), SHMBs with an affinity to boninite (Peng et al., 2013), and oceanic slab-derived melts including low-Mg and high-Mg adakitic rocks (Peng et al., 2012) within the TSGT. Most recently, Wan et al. (2010, 2012c) ascribed an arc environment to produce these late Neoarchean igneous rocks, based on the spatial distribution of late Neoarchean gabbroic, dioritic and granitic rocks.

In this study, the identification of high-K calc-alkaline, high Ba–Sr granites in the TSGT at 2.54–2.47 Ga, provides further constraints on the nature of events and overall crustal dynamics in the late Neoarchean. There is a consensus that high Ba–Sr granites are generally emplaced in extensional or non-compressional tectonic settings, such as during lithospheric extension, slab breakoff, or late- to post-orogenic gravitational collapse following an episode of crustal thickening (e.g., Qian et al., 2003; Fowler et al., 2008; Ye et al., 2008; Choi et al., 2009). These events may follow a period of subduction. Indeed, a subduction-related arc setting has previously been suggested to account for the genesis of high Ba–Sr granite (e.g., Tarney and Jones, 1994; Fowler and Henney, 1996; Fowler et al., 2001, 2008). The presence of contemporaneous slab melts (adakitic rocks, Peng et al., 2012) and sub-arc enriched mantle-derived sanukitoid magma and SHMBs with a boninite affinity (Wang et al., 2009; Peng et al., 2013), coupled with coeval high-Mg adakitic rocks representing the products of interaction between slab-derived melts and overlying peridotite mantle (Peng et al., 2012), is a strong argument in favor of active subduction at this time in the TSGT. Such a scenario would result from mantle enrichment beneath the TSGT. Hence, a subduction-related arc source is a plausible way to explain the generation of high Ba–Sr granites, which is also in agreement with the petrogenesis of the late Archean sanukitoids, SHMBs and adakitic rocks (Wang et al., 2009; Peng et al., 2012) in the study area. Importantly, ~2.6–2.5 Ga komatiitic rocks have so far not been discovered in the study area. It seems likely, therefore, that there was a change in regional tectonics from a plume-dominated regime at 2.71 Ga that resulted in komatiite and the scenario at 2.6–2.5 Ga that produced the range of rocks, including high Ba–Sr granites, with an arc signature. Furthermore, the following lines of evidence in the TSGT are also difficult to explain by a ~2.5 Ga mantle plume. For instance, 1) magmatic rocks of different ages and compositions occur in different zones and show an asymmetrical distribution; 2) the older rocks (2560–2525 Ma) commonly underwent stronger deformation and metamorphism than the younger rocks (2525–2480 Ma) (Wan et al., 2010); and 3) the lack of coeval voluminous basalts and radiating dike swarms. Accordingly, an active subduction environment can best explain the rock association and spatial distribution of the late Neoarchean igneous rocks discussed here.

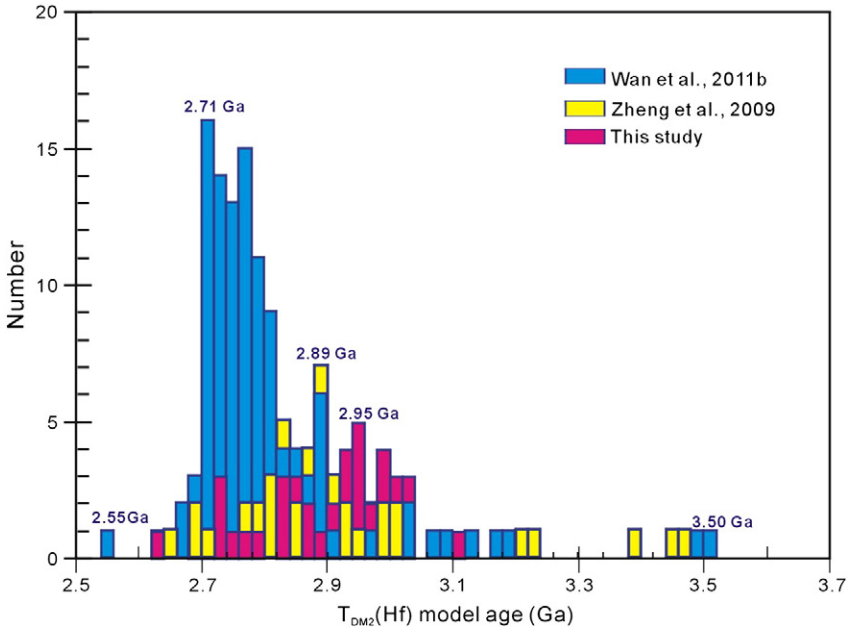

Fig. 15. Distribution of T_{DM2}(Hf) model ages of zircons in the TSGT.

5.5. Continental crustal growth and crustal evolution

It is generally considered that at least 70% of continental crust had been formed before the end of the Archean, with a striking global peak of rapid juvenile crustal generation at ~2.7 Ga (Hawkesworth and Kemp, 2006b,c; López et al., 2006; Kemp et al., 2007; Hawkesworth et al., 2010), although the mechanism with respect to plume or slab subduction is controversial (e.g., Stein and Hofmann, 1994; Martin, 1999; Smithies, 2000; Martin et al., 2005). The earliest generation of continental crust can be traced back to at least ~4.3 Ga as evidenced by Wilde et al. (2001). Indeed, evidence suggests that continental crustal growth was not continuous but episodic in the Archean (Albarede, 1998; Condie, 2000; Rino et al., 2004; Hawkesworth and Kemp, 2006b,c; Kemp et al., 2007). For the NCC, rapid crustal growth at ~2.7 Ga has been well established for the entire craton (e.g., Wu et al., 2005b; Wan et al., 2011). However, distinct from other cratons, such as the Superior (Percival et al., 2001), the western Canada Shield (Sandeman et al., 2006), Wyoming (Rino et al., 2004), the Baltic Shield (Bibikova et al., 2005; Halla, 2005; Samsonov et al., 2005), southern West Greenland (Thrane, 2002; Steenfelt et al., 2005), the Pilbara and Yilgarn cratons of Western Australia (Bateman et al., 2001; Blake, 2001; Rasmussen et al., 2005), southern Africa (Poujol et al., 2003) and Zimbabwe (Matthew et al., 1999; Hofmann et al., 2004), about 80% of the exposed igneous rocks in the NCC are ~2.5 Ga TTGs and associated rocks (Zhao et al., 2001, 2002; Wilde et al., 2005). Moreover, the imprint of a major 2.5 Ga tectono-thermal event was particularly strong in the NCC (Zhao et al., 2005; Wan et al., 2012c, and references therein). Although multiple tectono-thermal events have been revealed by the diverse chemistry of supracrustal and intrusive rock associations, zircon dating and Hf and Nd isotope studies (Zhao et al., 2012 and references therein), most magmatic events older than 2.8 Ga are reported only from the Eastern Block of the NCC (Liu et al., 1992; Song et al., 1996; Wan et al., 2012a and references therein).

The oldest rocks and zircons (~3.8 Ga) discovered in the Eastern Block are the result of reworking of juvenile crust based on their elevated $\delta^{18}O$ values (e.g., Wilde et al., 2008), indicating that the earliest crustal differentiation took place before ~3.8 Ga. Other 3.8–3.1 Ga tectono-magmatic events have been revealed from trondhjemitic rocks (3.8–3.4 Ga), mafic dykes (3.31 Ga), felsic veins (3.6–3.3 Ga) and monzogranite (3.1 Ga) in the Anshan area within the Eastern Block (Liu et al., 2008; Wan et al., 2012a). Episodes of granitic magmatism younger than 3.0 Ga are also reported, including the ~3.0 Ga Anshan and Tiejiashan granites (Liu et al., 1992; Song et al., 1996). Moreover, two major mantle depletion events (at ~3.4 Ga and 2.8 Ga) have also been documented on the basis of the integration of two-stage Nd model ages (T_{DM2}) (Wu et al., 2005a), which correspond to crustal formation at these times. This suggests that juvenile continental crustal growth was the result of multiple episodes of magmatic extraction from the mantle, accompanied by episodic crustal reworking. Nonetheless, in the case of the TSGT where the greenstones are well preserved (Jahn, et al., 1988; Polat et al., 2006), rocks with an emplacement age >2.8 Ga have not been reported so far and magmatic events >2.8 Ga are only revealed from a few inherited zircons, including 3.6 Ga and ~2.85 Ga inherited zircons from granite in the Taishan complex (Lu et al., 2008), and the 2837 ± 10 Ma inherited zircons from the Yishui adakitic intrusions (Peng et al., 2012). Our whole-rock Nd model ages and zircon Hf model ages of the high Ba–Sr granites, in combination with zircon Hf model ages reported recently from the TSGT (Zheng et al., 2009; Wan et al., 2011), demonstrate that crustal basement >2.8 Ga is present in the area, and that the oldest crustal rocks might have been emplaced at ~3.5 Ga (Fig. 15), and that both extraction of new material from the mantle and reworking of older crust were important for the secular evolution of continental crust in the TSGT. On the other hand, the marked depletion evident in most zircon Hf and whole-rock Nd isotopic compositions of the ~2.6–2.5 Ga igneous rocks indicates that their parental magmas were derived from a highly depleted juvenile source (Jahn et al., 1988; Cao et al., 1996; Polat et al., 2006; Yang et al., 2008; Wang et al., 2009; Wan et al., 2011). This also indicates that, apart from the mantle-derived mafic–ultramafic rocks (i.e., gabbros (Wan et al., 2010), and the SHMBs (Peng et al., 2013), the addition of minor ~2.6–2.5 Ga intermediate-felsic igneous rocks [i.e., sanukitoids (Wang et al., 2009) and high Ba–Sr granites (this study)] that originated from the re-enriched mantle, also made an important contribution to crustal evolution during the late Neoarchean, even though most of ~2.5 Ga granitic rocks resulted from reworking of older continental crust (e.g., Yang et al., 2008; Wan et al., 2011).

6. Conclusions

Geochronological, geochemical and zircon Hf isotopic data for the late Neoarchean potassic high Ba–Sr granites in the Taishan granite–

greenstone terrane (TSGT), Eastern Block of the North China Craton, allow us to reach the following conclusions:

(1) These high Ba–Sr granites were emplaced at ~2.54 Ga (Wanghailou), ~2.52 Ga (Hujiazhuang) and ~2.47 Ga (Xiajiazhuang), respectively.
(2) They were derived from a highly enriched mantle source that was metasomatized by subduction-related fluids and/or melts prior to extraction and the resultant magmas experienced some degrees of crustal contamination during ascent.
(3) An active subduction environment is the most viable tectonic setting for their generation, rather than a mantle plume.
(4) A crustal basement >2.8 Ga was present in the area, and both extraction of new material from the mantle and reworking of older crust were important for the secular evolution of continental crust in the TSGT.

Acknowledgments

We acknowledge Dr. D-S. Zhang for his help during the fieldwork and Y. Liu, L. Qi, L.-Y. Ma and Y.-F. Cai for their assistance during geochemical, LA-ICP-MS dating and zircon Hf analyses. We also thank two anonymous reviewers and editor Klaus Mezger for their constructive comments. This research was supported by the Natural Science Foundation of China (grant nos. 40703007, 40972046, 41172095 and 41272126), the Chinese Academy of Sciences (GIGCX-08-02 and GIGCAS-135-Y234151001) and the China Scholarship Council (file no. 2010491212). This is a contribution from the Guangzhou Institute of Geochemistry, Chinese Academy of Sciences (GIG, CAS; no. 1637) and the Institute for Geoscience Research (TIGeR; no. 449).

References

Albarede, F., 1998. The growth of continental crust. Tectonophysics 296, 1–14.
Aldanmaz, E., Pearce, J.A., Thirlwall, M.F., Mitchell, J.G., 2000. Petrogenetic evolution of Late Cenozoic, post-collision volcanism in western Anatolia, Turkey. Journal of Volcanology and Geothermal Research 102, 67–95.
Amelin, Y., Lee, D.C., Halliday, A.N., Pidgeon, R.T., 1999. Nature of the Earth's earliest crust from hafnium isotopes in single detrital zircons. Nature 399, 252–255.
Anderson, T., 2002. Correction of common lead in U–Pb analyses that do not report ^{204}Pb. Chemical Geology 192, 59–79.
Barbarin, B., 1999. A review of the relationships between granitoids types, their origins and their geodynamic environments. Lithos 46, 605–626.
Bateman, R., Costa, S., Swe, T., Lambert, D., 2001. Archaean mafic magmatism in the Kalgoorlie area of the Yilgarn Craton, western Australia: a geochemical and Nd isotopic study of the petrogenetic and tectonic evolution of a greenstone belt. Precambrian Research 108, 75–112.
Bibikova, E.V., Petrova, A., Claesson, S., 2005. The temporal evolution of sanukitoids in the Karelian Craton, Baltic Shield: an ion microprobe U–Th–Pb isotopic study of zircons. Lithos 79, 129–145.
Blake, T.S., 2001. Cyclic continental mafic tuff and flood basalt volcanism in the Late Archaean Nullagine and Mount Jope Supersequences in the eastern Pilbara, western Australia. Precambrian Research 107, 139–177.
Blichert-Toft, J., Albarede, F., 1997. The Lu–Hf geochemistry of chondrites and the evolution of the mantle–crust system. Earth and Planetary Science Letters 148, 243–258.
Canning, J.C., Henney, P.J., Morrison, M.A., Gaskarth, J.W., 1996. Geochemistry of late Caledonian minettes from northern Britain: implications for the Caledonian subcontinental lithospheric mantle. Mineralogical Magazine 60, 221–236.
Cao, G., Wang, Z., Cheng, Z., Dong, Y., Li, P., Wang, S., Jin, L., Shen, K., Xu, J., Shen, K., Shi, Y., Xu, H., Zhan, C., Zheng, L., Zhang, Z., Ren, X., Zai, Y., Ma, Y., Liang, B., 1996. Early Precambrian Geology of Western Shandong. Geological Publishing House, Beijing, pp. 1–210 (in Chinese with English Abstract).
Castro, A., 2004. The source of granites: inferences from the Lewisian complex. Scottish Journal of Geology 40, 49–65.
Chappell, B.W., White, A.J.R., 1992. I- and S- type granites in Lachlan Fold Belt. Transactions Royal Society Edinburgh 83, 1–26.
Chappell, B.W., White, A.J.R., 2001. Two contrasting granitic types: 25 years later. Australian Journal of Earth Sciences 48 (4), 489–500.
Chebeu, C., Nlend, C.D.N., Nzenti, J.P., Ganno, S., 2011. Neoproterozoic high-K calc-alkaline granitoids from Bapa-Batié, North Equatorial Fold Belt, Central Cameroon: petrogenesis and geodynamic significance. The Open Geology Journal 5, 1–20.
Cheng, S.H., Kusky, T., 2007. Komatiites from west Shandong, North China craton: implications for plume tectonics. Gondwana Research 12, 77–83.
Choi, S.G., Rajesh, V.J., Seo, J., Park, J.W., Oh, C.W., Pak, S.J., Kim, S.W., 2009. Petrology, geochronology and tectonic implications of Mesozoic high Ba–Sr granites in the Haemi area, Hongseong Belt, South Korea. Island Arc 18, 266–281.
Chu, N.C., Taylor, R.N., Chavagnac, V., Nesbitt, R.W., Boella, R.M., Milton, J.A., Germain, C.R., Bayon, G., Burton, K., 2002. Hf isotope ratio analysis using multicollector inductively coupled plasma mass spectrometry: an evaluation of isobaric interference corrections. Journal of Analytical Atomic Spectrometry 17, 1567–1574.
Condie, K.C., 2000. Episodic continental growth models: after thoughts and extensions. Tectonophysics 322, 153–162.
Condie, K.C., 2005. TTGs and adakites: are they both slab melts? Lithos 80, 33–44.
de Oliveira, M.A., Dall'Agnol, R., Althoff, F.J., Leite, A.A.S., 2009. Mesoarchean sanukitoid rocks of the Rio Maria Granite–greenstone Terrane, Amazonian craton, Brazil. Journal of South American Earth Sciences 27, 146–160.
de Oliveira, M.A., Dall'Agnol, R., Scaillet, B., 2010. Petrological constraints on crystallization conditions of mesoarchean sanukitoid rocks, Southeastern Amazonian Craton, Brazil. Journal of Petrology 51, 2121–2148.
De, B.P., Taylor, P.D.P., 1993. Table of the isotopic compositions of the elements. International Journal of Mass Spectrometry 123, 149–166.
Defant, M.J., Drummond, M.S., 1990. Derivation of some modern arc magmas by melting of young subducted oceanic lithosphere. Nature 347, 662–665.
Defant, M.J., Clark, L.F., Stewart, R.H., Drummond, M.S., De Boer, J.Z., Maury, R.C., Bellon, H., Jackson, T.E., Restrepo, J.F., 1991a. Andesite and dacite genesis via contrasting processes: the geology and geochemistry of El Valle Volcano, Panama. Contributions to Mineralogy and Petrology 106, 309–324.
Defant, M.J., Richerson, P.M., De Boer, J.Z., Stewart, R.H., Maury, R.C., Bellon, H., Drummond, M.S., Feigenson, M.D., Jackson, T.E., 1991b. Dacite genesis via both slab melting and differentiation: petrogenesis of La Yeguada volcanic complex, Panama. Journal of Petrology 32, 1101–1142.
Drummond, M.S., Defant, M.J., 1990. A model for trondhjemite–tonalite–dacite genesis and crustal growth via slab melting: Archaean to modern comparisons. Journal of Geophysical Research 95, 21503–21521.
El Bouseily, A.M., El Sokkary, A.A., 1975. The relation between Rb, Ba and Sr in granitic rocks. Chemical Geology 16, 207–219.
Fowler, M.B., Henney, P.J., 1996. Mixed Caledonian appinite magmas: implications for lamprophyre fractionation and high Ba–Sr granite genesis. Contributions to Mineralogy and Petrology 126, 199–215.
Fowler, M.B., Henney, P.J., Darbyshire, D.P.F., Greenwood, P.B., 2001. Petrogenesis of high Ba–Sr granites: the Rogart pluton, Sutherland. Journal of the Geological Society of London 158, 521–534.
Fowler, M.B., Kocks, H., Darbyshire, D.P.F., Greenwood, P.B., 2008. Petrogenesis of high Ba–Sr plutons from the Northern Highlands Terrane of the British Caledonian Province. Lithos 105, 129–148.
Frost, C.D., Frost, B.R., Chamberlain, K.R., Hulsebosch, T.P., 1998. The late Archaean history of the Wyoming province as recorded by granitic magmatism in the Wind River Range, Wyoming. Precambrian Research 89, 145–173.
Frost, B.R., Arculus, R.J., Barnes, C.G., Collins, W.J., Ellis, D.J., Frost, C.D., 2001. A geochemical classification of granitic rock suites. Journal of Petrology 42, 2033–2048.
Green, D.H., Wallace, M.E., 1988. Mantle metasomatism by ephemeral carbonatite melts. Nature 336, 459–462.
Griffin, W.L., Pearson, N.J., Elusive, E., Jackson, S.E., van Achtenberg, E., O'Reilly, S.Y., She, S.R., 2000. The Hf isotope composition of carbonic mantle: LAM-MC-ICPMS analysis of zircon megacrysts in kimberlites. Geochimica et Cosmochimica Acta 64, 133–147.
Griffin, W.L., Wang, X., Jackson, S.E., Pearson, N.J., O'Reilly, S.Y., Xu, X., Zhou, X., 2002. Zircon chemistry and magma mixing, SE China: in-situ analysis of Hf isotopes, Pingtan and Tonglu igneous complexes. Lithos 61, 237–269.
Halla, J., 2005. Late Archean high-Mg granitoids (sanukitoids) in the southern Karelian domain, eastern Finland: Pb and Nd isotopic constraints on crust–mantle interactions. Lithos 79, 161–178.
Hawkesworth, C.J., Kemp, A.I.S., 2006a. Using hafnium and oxygen isotopes in zircon to unravel the record of crustal evolution. Chemical Geology 226, 144–162.
Hawkesworth, C.J., Kemp, A.I.S., 2006b. Evolution of the continental crust. Nature 443, 811–817.
Hawkesworth, C.J., Kemp, A.I.S., 2006c. The differentiation and rates of generation of the continental crust. Chemical Geology 226, 134–143.
Hawkesworth, C.J., Dhuime, B., Pietranik, A., Cawood, P., Kemp, A.I.S., Storey, C., 2010. The generation and evolution of the continental crust. Journal of the Geological Society of London 167, 229–248.
Hofmann, A., Dirks, P.H.G.M., Jelsma, H.A., 2004. Clastic sedimentation in a late Archaean accretionary terrane, Midlands greenstone belt, Zimbabwe. Precambrian Research 129, 47–69.
Hou, G.T., Wang, C.C., Wang, Y.X., Xiao, F.F., Li, L., 2008. SHRIMP zircon U–Pb chronology and tectonic significance of the latest Neoarchean Mengshan diorite, Western Shandong Province. Geological Journal of China Universities 14 (3), 22–28.
Hu, Z.C., Liu, Y.S., Chen, L., Zhou, L., Li, M., Zong, K.Q., Zhu, L.Y., Gao, S., 2011. Contrasting matrix induced elemental fractionation in NIST SRM and rock glasses during laser ablation ICP-MS analysis at high spatial resolution. Journal of Analytical Atomic Spectrometry 26 (2), 425–430.
Ionov, D.A., Dupuy, C., O'Reilly, S.Y., Kopylova, M.G., Genshaft, Y., 1993. Carbonate peridotite xenoliths from Spitsbergen: implications for trace element signature of carbonate mantle metasomatism. Earth and Planetary Science Letters 119, 283–297.
Ionov, D.A., O'Reilly, S.Y., Griffin, W.L., 1997. Volatile-bearing minerals and lithophile trace elements in the upper mantle. Chemical Geology 141, 153–184.
Jahn, B.M., Condie, K.C., 1995. Evolution of the Kaapvaal Craton as viewed from geochemical and Sm-Nd isotopic analyses of intracratonic pelites. Geochimica et Cosmochimica Acta 59, 2239–2258.

Jahn, B.M., Auvray, B., Shen, Q.H., Liu, D.Y., Zhang, Z.Q., 1988. Archean crustal evolution in China: the Taishan complex, and evidence for juvenile crustal addition from long-term depleted mantle. Precambrian Research 38, 381–403.
Jayananda, M., Martin, H., Peucat, J.-J., Mahabaleswar, B., 1995. Late Archaean crust–mantle interactions: geochemistry of LREE-enriched mantle derived magmas. Example of the Closepet batholith, Southern India. Contributions to Mineralogy and Petrology 199, 314–329.
Jayananda, M., Moyen, J.F., Martin, H., Peucat, J.J., Auvray, B., Mahabaleswar, B., 2000. Late Archaean (2550–2520 Ma) juvenile magmatism in the eastern Dharwar craton, southern India: constraints from geochronology, Nd–Sr isotopes and whole rock geochemistry. Precambrian Research 99, 225–254.
Jiang, N., Guo, J.H., Zhai, M.G., Zhang, S.Q., 2010. Similar to 2.7 Ga crust growth in the North China craton. Precambrian Research 179, 37–49.
Kemp, A.I.S., Hawkesworth, C.J., 2003. Granitic perspectives on the generation and secular evolution of the continental crust. In: Eiler, J. (Ed.), Treatise on Geochemistry, 3.11. Elsevier, New York, pp. 349–410.
Kemp, A.I.S., Hawkesworth, C.J., Paterson, B.A., Kinny, P.D., 2006. Episodic growth of the Gondwana supercontinent from hafnium and oxygen isotopes in zircon. Nature 439, 580–583.
Kemp, A.I.S., Hawkesworth, C.J., Foster, G.L., Paterson, B.A., Woodhead, J.D., Hergt, J.M., Gray, C.M., Whitehouse, M.J., 2007. Magmatic and crustal differentiation history of granitic rocks from Hf–O isotopes in zircon. Science 315, 980–983.
Kemp, A.I.S., Hawkesworth, C.J., Collins, W.J., Gray, C.M., EIMF, 2009. Isotopic evidence for rapid continental growth in an extensional accretionary orogen: the Tasmanides, eastern Australia. Earth and Planetary Science Letters 285, 455–466.
Kepezhinskas, P., McDermott, F., Defant, M.J., Hochstaedter, A., Drummond, M.S., 1997. Trace element and Sr–Nd–Pb isotopic constraints on a three-component model of Kamchatka Arc petrogenesis. Geochimica et Cosmochimica Acta 61 (3), 577–600.
Keto, L.S., Jacobsen, S.B., 1987. Nd and Sr isotopic variations of Early Paleozoic oceans. Earth and Planetary Science Letters 84, 27–41.
Kilian, R., Stern, C.R., 2002. Constraints on the interaction between slab melts and the mantle wedge from adakitic glass in peridotites xenoliths. European Journal of Mineralogy 14, 25–36.
Kleinhanns, I.C., Kramers, J.D., Kamber, B.S., 2003. Importance of water for Archean granitoid petrology: a comparative study of TTG and potassic granitoids from Barberton Mountain Land, South Africa. Contributions to Mineralogy and Petrology 145, 377–389.
Kovalenko, A., Clemens, J.D., Savatenkov, V., 2005. Petrogenetic constraints for the genesis of Archaean sanukitoid suites: geochemistry and isotopic evidence from Karelia, Baltic Shield. Lithos 79, 147–160.
Kröner, A., Wilde, S.A., Zhao, G.C., O'Brien, P.J., Sun, M., Liu, D.Y., Wan, Y.S., Liu, S.W., Guo, J.H., 2006. Zircon geochronology and metamorphic evolution of mafic dykes in the Hengshan Complex of northern China: evidence for late Palaeoproterozoic extension and subsequent high-pressure metamorphism in the North China Craton. Precambrian Research 146, 45–67.
LaFlèche, M.R., Camire, G., Jenner, G.A., 1998. Geochemistry of post-Acadian, Carboniferous continental intraplate basalts from the Maritimes Basin, Magdalen islands, Quebec, Canada. Chemical Geology 148, 115–136.
Larionova, Y.U., Samsonov, A.V., Shatagin, K.N., 2007. Source of Archean sanukitoids (high-Mg subalkaline granitoids) in the Karelian craton: Sm–Nd and Rb–Sr isotopic-geochemical evidence. Petrology 15, 530–593.
Li, S.Z., Zhao, G.C., 2007. SHRIMP U–Pb zircon geochronology of the Liaoji granitoids: constraints on the evolution of the Paleoproterozoic Jiao-Liao-Ji belt in the Eastern Block of the North China Craton. Precambrian Research 158, 1–16.
Li, S.Z., Zhao, G.C., Sun, M., Han, Z.Z., Luo, Y., Hao, D.F., Xia, X.P., 2005. Deformation history of the Paleoproterozoic Liaohe assemblage in the eastern block of the North China Craton. Journal of Asian Earth Sciences 24, 659–674.
Li, S.Z., Zhao, G.C., Sun, M., Han, Z.Z., Zhao, G.T., Hao, D.F., 2006. Are the South and North Liaohe Groups of the North China Craton different exotic terranes? Nd isotope constraints. Gondwana Research 9, 198–208.
Li, T.S., Zhai, M.G., Peng, P., Chen, L., Guo, J.H., 2010. Ca. 2.5 billion year old coeval ultramafic–mafic and syenitic dykes in Eastern Hebei: implications for cratonization of the North China Craton. Precambrian Research 180, 143–155.
Liu, D.Y., Nutman, A.P., Compston, W., Wu, J.S., Shen, Q.H., 1992. Remnants of 3800 Ma crust in the Chinese part of the Sino-Korean Craton. Geology 20, 339–342.
Liu, S.W., Zhao, G.C., Wilde, S.A., Shu, G.M., Sun, M., Li, Q.G., Tian, W., Zhang, J., 2006. Th-U-Pb monazite geochronology of the Lüliang and Wutai Complexes: constraints on the tectonothermal evolution of the Trans-North China Orogen. Precambrian Research 148, 205–225.
Liu, D.Y., Wilde, S.A., Wan, Y.S., Wu, J.S., Zhou, H.Y., Dong, C.Y., Yin, X.Y., 2008. New U–Pb and Hf isotopic data confirm Anshan as the oldest preserved segment of the North China Craton. American Journal of Science 308, 200–231.
Liu, Y.S., Gao, S., Hu, Z.C., Gao, C.G., Zong, K.Q., Wang, D.B., 2010a. Continental and oceanic crust recycling-induced melt–peridotite interactions in the Trans-North China Orogen: U–Pb dating, Hf isotopes and trace elements in zircons from mantle xenoliths. Journal of Petrology 51 (1–2), 537–571.
Liu, Y.S., Hu, Z.C., Zong, K.Q., Zong, K.Q., Gao, C.G., Gao, S., Xu, J., Chen, H.H., 2010b. Reappraisement and refinement of zircon U–Pb isotope and trace element analyses by LA-ICP-MS. Chinese Science Bulletin 55 (15), 1535–1546.
Lobach-Zhuchenko, S.B., Rollinson, H., Chekulaev, V.P., Arestova, N.A., Kovalenko, A.V., Ivanikov, V.V., Guseva, N.S., Sergeev, S.A., Matukov, D.I., Jarvis, K.E., 2005. The Archaean sanukitoid series of the Baltic shield—geological setting, geochemical characteristics and implications for their origin. Lithos 79, 107–128.
Lobach-Zhuchenko, S.B., Rollinson, H., Chekulaev, V.P., Savatenkov, V.M., Kovalenko, H., Martin, A.V., Guseva, N.S., Arestova, N.A., 2008. Petrology of a Late Archaean, highly potassic, sanukitoid pluton from the Baltic Shield: insights into late Archaean mantle metasomatism. Journal of Petrology 49 (3), 393–420.
López, S., Fernandez, C., Castro, A., 2006. Evolution of the Archaean continental crust: insights from the experimental study of Archaean granitoids. Current Science 91, 607–621.
Lu, S.N., Chen, Z.H., Xiang, Z.Q., 2008. Geochronological Framework of Ancient Intrusions in Taishan Geopark, China. Geological Publishing House, Beijing, pp. 1–90.
Ludwig, K.R., 2003. Users manual for Isoplot 3.00: a geochronological toolkit for Microsoft Excel. Berkeley Geochronology Center, Special Publication, No. 4.
Luo, Y., Sun, M., Zhao, G.C., Li, S.Z., Xu, P., Ye, K., Xia, X.P., 2004. LA-ICP-MS U–Pb zircon ages of the Liaohe Group in the Eastern Block of the North China Craton: constraints on the evolution of the Jiao-Liao-Ji Belt. Precambrian Research 134, 349–371.
Luo, Y., Sun, M., Zhao, G.C., Ayers, J.C., Li, S.Z., Xia, X.P., Zhang, J.H., 2008. A comparison of U–Pb and Hf isotopic compositions of detrital zircons from the North and South Liaohe Group: constraints on the evolution of the Jiao-Liao-Ji Belt, North China Craton. Precambrian Research 163, 279–306.
Maniar, P.D., Piccoli, P.M., 1989. Tectonic discrimination of granitoids. Geological Society of America Bulletin 101, 635–643.
Martin, H., 1994. The Archean grey gneisses and the genesis of continental crust. In: Condie, K.C. (Ed.), Archaean Crustal Evolution: Developments in Precambrian Geology. Elsevier, Amsterdam, pp. 205–259.
Martin, H., 1999. Adakitic magmas: modern analogues of Archaean granitoids. Lithos 26, 411–429.
Martin, H., Smithies, R.H., Rapp, R., Moyen, J.F., Champion, D., 2005. An overview of adakite, tonalite–trondhjemite–granodiorite (TTG), and sanukitoid: relationships and some implications for crustal evolution. Lithos 79, 1–24.
Martin, H., Moyen, J.-F., Rapp, R., 2009. Sanukitoids and the Archaean–Proterozoic boundary. Transactions of the Royal Society of Edinburgh-Earth Sciences 100, 15–33.
Matthew, S.A., Robert, W.N., Stephen, R., James, F., 1999. U–Pb zircon evidence for an extensive early Archean craton in Zimbabwe: a reassessment of the timing of craton formation, stabilization, and growth. Geology 27, 707–710.
Maury, R.C., Sajona, F.G., Pubellier, M., Bellon, H., Defant, M.J., 1996. Fusion de la croute océanique dans les zones de subduction/collision récentes: l'exemple de Mindanao (Philippines). Bulletin de la Société Géologique de France 167, 579–595.
Morris, P.A., 1995. Slab melting as an explanation of Quaternary volcanism and aseismicity in southwest Japan. Geology 23, 395–398.
Moyen, J.-F., 2011. The composite Archaean grey gneisses: petrological significance, and evidence for a non-unique tectonic setting for Archaean crustal growth. Lithos 123, 21–36.
Moyen, J.-F., Martin, H., Jayananda, M., 2001. Multi-element geochemical modelling of crust–mantle interactions during late-Archaean crustal growth: the Closepet granite (South India). Precambrian Ressearch 112, 87–105.
Moyen, J.-F., Martin, H., Jayananda, M., Auvray, B., 2003. Late Archaean granites: a typology based on the Dharwar Craton (India). Precambrian Research 127, 103–123.
Nowell, G.M., Kempton, P.D., Noble, S.R., Fitton, J.G., Saunders, A.D., Mahoney, J.J., Taylor, R.N., 1998. High precision Hf isotope measurements of MORB and OIB by thermal ionisation mass spectrometry: insights into the depleted mantle. Chemical Geology 149, 211–233.
Nutman, A.P., Wan, Y.S., Du, L.L., Friend, C.R.L., Dong, C.Y., Xie, H.Q., Wang, W., Sun, H.Y., Liu, D.Y., 2011. Multistage late Neoarchaean crustal evolution of the North China Craton, eastern Hebei. Precambrian Research 189, 43–65.
Peccerillo, A., Taylor, S.R., 1976. Geochemistry of Eocene calc-alkaline volcanic rocks from the Kastamonu Area, Northern Turkey. Contributions to Mineralogy and Petrology 58, 63–81.
Peng, T.P., Fan, W.M., Peng, B.X., 2012. Geochronology and geochemistry of late Archean adakitic plutons from the Taishan granite–greenstone Terrain: implications for tectonic evolution of the eastern North China Craton. Precambrian Research 208–211, 53–71.
Peng, T.P., Wilde, S.A., Fan, W.M., Peng, B.X., 2013. Late Archaean siliceous high magnesian basalt (SHMB) from the Taishan Greenstone Terrane, Eastern North China Craton: petrogenesis and tectonic implications. Precambrian Research 228, 233–249.
Percival, J.A., Stern, R.A., Skulski, T., 2001. Crustal growth through successive arc magmatism: reconnaissance U–Pb SHRIMP data from the northeastern Superior Province, Canada. Precambrian Research 109, 203–238.
Petford, N., Atherton, M., 1996. Na-rich partial melts from newly underplated basaltic crust: the Cordillera Blanca Batholith, Peru. Journal of Petrology 37, 1491–1521.
Plank, T., Langmuir, C.H., 1998. The geochemical composition of subducting sediment and its consequences for the crust and mantle. Chemical Geology 145, 325–344.
Polat, A., Li, J., Fryer, B., Kusky, T., Gagnon, J., Zhang, S., 2006. Geochemical characteristics of the Neoarchean (2800–2700 Ma) Taishan greenstone belt, North China Craton: evidence for plume–craton interaction. Chemical Geology 230, 60–87.
Poujol, M., Robb, L.J., Anhaeusser, C.R., Gericke, B., 2003. A review of the geochronological constraints on the evolution of the Kaapvaal Craton, South Africa. Precambrian Research 127, 181–213.
Prouteau, G., Scaillet, B., Pichavant, M., Maury, R., 2001. Evidence for mantle metasomatism by hydrous silicic melts derived from subducted oceanic crust. Nature 410, 197–200.
Qi, L., Hu, J., Gregoire, D.C., 2000. Determination of trace elements in granites by inductively coupled plasma-mass spectrometry. Talanta 51, 507–513.
Qian, Q., Chung, S.L., Lee, T.Y., Wen, D.J., 2003. Mesozoic high Ba–Sr granitoids from North China: geochemical characteristics and geological implications. Terra Nova 15, 272–278.

Rapp, R.P., Watson, E.B., 1995. Dehydration melting of metabasalt at 8–32 kbar: implications for continental growth and crust–mantle recycling. Journal of Petrology 36, 891–931.
Rapp, R.P., Shimizu, N., Norman, M.D., Applegate, G.S., 1999. Reaction between slab-derived melts and peridotite in the mantle wedge: experimental constraints at 3.8 GPa. Chemical Geology 160, 335–356.
Rapp, R.P., Xiao, L., Shimizu, N.M., 2002. Experimental constraints on the origin of potassium-rich adakities in east China. Acta Petrologica Sinica 18, 293–311.
Rasmussen, B., Blake, T.S., Fletcher, I.R., 2005. U–Pb zircon age constraints on the Hamersley spherule beds: evidence for a single 2.63 Ga Jeerinah–Carawine impact ejecta layer. Geology 33, 725–728.
Rino, S., Komiya, T., Windley, B.F., Katayama, I., Motoki, A., Hirata, T., 2004. Major episodic increases of continental crustal growth determined from zircon ages of river sands; implications for mantle overturns in the Early Precambrian. Physics of the Earth and Planetary Interiors 146, 369–394.
Rudnick, R.L., 1995. Making continental crust. Nature 378, 571–578.
Rudnick, R.L., McDonough, W.F., Chappel, B.W., 1993. Carbonatite metasomatism in the northern Tanzania mantle: petrographic and geochemical characteristics. Earth and Planetary Science Letters 114, 463–475.
Sajona, F.G., Maury, R.C., Bellon, H., Cotton, J., Defant, M.J., Pubellier, M., 1993. Initiation of subduction and the generation of slab melts in western and eastern Mindanao, Philippines. Geology 21, 1007–1010.
Sajona, F.G., Bellon, H., Maury, R.C., Pubellier, M., Cotton, J., Rangin, C., 1994. Magmatic response to abrupt changes in geodynamic settings: Pliocene–Quaternary calc-alkaline and Nb-enriched lavas from Mindanao (Philippines). Tectonophysics 237, 47–72.
Samsonov, A.V., Bogina, M.M., Bibikova, E.V., Petrova, A.Yu., Shchipansky, A.A., 2005. The relationship between adakitic, calc-alkaline volcanic rocks and TTGs: implications for the tectonic setting of the Karelian greenstone belts, Baltic Shield. Lithos 79, 83–106.
Sandeman, H.A., Hanmer, S., Tella, S., Armitage, A.A., Davis, W.J., Ryan, J.J., 2006. Petrogenesis of Neoarchean volcanic rocks of the MacQuoid supracrustal belt: a back-arc setting for the northwestern Hearne subdomain, western Churchill Province, Canada. Precambrian Research 144, 140–165.
Scambelluri, M., Philippot, P., 2001. Deep fluids in subduction zones. Lithos 55, 213–227.
Scherer, E., Munker, C., Mezger, K., 2001. Calibration of the lutetium–hafnium clock. Science 293, 683–687.
Schiano, P., Clochiatti, R., Shimizu, N., Maury, R.C., Jochum, K.P., Hofman, A.W., 1995. Hydrous, silica-rich melts in the sub-arc mantle and their relationships with erupted arc lavas. Nature 377, 595–600.
Schmidt, M.W., Poli, S., 1998. Experimentally based water budgets for dehydrating slabs and consequences for arc magma generation. Earth and Planetary Science Letters 163, 361–379.
Shen, Q.H., Song, B., Xu, H.F., Geng, Y.S., Shen, K., 2004. Emplacement and metamorphism ages of the Caiyu and Dashan igneous bodies, Yishui County, Shandong Province: zircon SHRIMP chronology. Geological Review 50, 275–284 (in Chinese with English abstract).
Shen, Q.H., Zhao, Z.R., Song, H.X., 2007. Geology, Petrochemistry and SHRIMP zircon U–Pb dating of the Mashan and Xueshan granitoids in Yishui County, Shandong Province. Geological Review 53, 180–186 (in Chinese with English abstract).
Shimoda, G., Tatsumi, Y., Nohda, S., Ishizaka, K., Jahn, B.M., 1998. Setouchi high-Mg andesites revisited: geochemical evidence for melting of subducting sediments. Earth and Planetary Science Letters 160, 479–492.
Smithies, R.H., 2000. The Archaean tonalite–trondhjemite–granodiorite (TTG) series is not an analogue of Cenozoic adakite. Earth and Planetary Science Letters 182, 115–125.
Smithies, R.H., Champion, D.C., 2000. The Archaean high-Mg diorite suite: links to tonalite–trondhjemite–granodiorite magmatism and implications for early Archaean crustal growth. Journal of Petrology 41 (12), 1653–1671.
Smithies, R.H., Champion, D.C., Sun, S.S., 2004. Evidence for Early LREE-enriched mantle source regions: diverse magmas from the c. 3.0 Ga Mallina Basin, Pilbara Craton, NW Australia. Journal of Petrology 45, 1515–1537.
Song, B., Nutman, A.P., Liu, D.Y., Wu, J.S., 1996. 3800 to 2500 Ma crustal evolution in the Anshan area of Liaoning Province, northeastern China. Precambrian Research 78, 79–94.
Souza, Z.S., Martin, H., Peucat, J.-J., Jardim de Sa, E.F., Macedo, M.H.F., 2007. Calc-alkaline magmatism at the Archean–Proterozoic transition: the Caico Complex Basement (NE Brazil). Journal of Petrology 48, 2149–2185.
Steenfelt, A., Garde, A.A., Moyen, J.-F., 2005. Mantle wedge involvement in the petrogenesis of Archaean grey gneisses in West Greenland. Lithos 79, 207–228.
Steiger, R.H., Jäger, E., 1977. Subcommission on geochronology: convention on the use of decay constants in geo- and cosmochronology. Earth and Planetary Science Letters 36, 359–362.
Stein, M., Hofmann, A.W., 1994. Mantle plumes and episodic crustal growth. Nature 372, 63–68.
Stern, C.R., Kilian, R., 1996. Role of the subducted slab, mantle wedge and continental crust in the generation of adakites from the Andean Austral Volcanic Zone. Contributions to Mineralogy and Petrology 123, 263–281.
Stevenson, R., Henry, P., Gariépy, C., 1999. Assimilation-fractional crystallization origin of Archean Sanukitoid Suites: western Superior Province, Canada. Precambrian Research 96, 83–99.
Streckeisen, A.L., 1976. Classification of the common igneous rocks by means of their chemical composition: a provisional attempt. Neues Jahrbuch fur Mineralogie, Monatshefte 1976 (H. 1), 1–15.
Sun, S.S., McDonough, W.F., 1989. Chemical and isotopic systematics of oceanic basalts: implication for mantle composition and processes. In: Sauders, A.D., Norry, M.J. (Eds.), Magmatism in the ocean basins. : Geol. Soc. Spe. Publ., 42. Blackwell Scientific Publications, London, pp. 313–345.
Sutcliffe, R.H., Smith, A.R., Doherty, W., Barnett, R.L., 1990. Mantle derivation of Archean amphibole-bearing granitoid and associated mafic rocks: evidence from the southern Superior Province, Canada. Contributions to Mineralogy and Petrology 105, 255–274.
Sylvester, P.J., 1994. Archaean granite plutons. In: Condie, K.C. (Ed.), Archaean crustal evolution. : Developments in Precambrian Geology, vol. 11. Elsevier, Amsterdam, pp. 261–314.
Tam, P.Y., Zhao, G.C., Liu, F.L., Zhou, X.W., Sun, M., Li, S.Z., 2011. SHRIMP U–Pb zircon ages of high-pressure mafic and pelitic granulites and associated rocks in the Jiaobei massif: constraints on the metamorphic ages of the Paleoproterozoic Jiao-Liao-Ji Belt in the North China Craton. Gondwana Research 19, 150–162.
Tam, P.Y., Zhao, G.C., Liu, F.L., Zhou, X.W., Sun, M., Li, S.Z., 2012a. Metamorphic P-T path and implications of high-pressure pelitic granulites from the Jiaobei massif in the Jiao-Liao-Ji Belt, North China Craton. Gondwana Research 22, 104–117.
Tam, P.Y., Zhao, G.C., Zhou, X.W., Guo, J.H., Sun, M., Li, S.Z., Yin, C.Q., Wu, M.L., 2012b. Metamorphic P-T path and tectonic implications of medium-pressure pelitic granulites from the Jiaobei massif in the Jiao-Liao-Ji Belt, North China Craton. Precambrian Research 220–221, 177–191.
Tarney, J., Jones, C.E., 1994. Trace element geochemistry of orogenic igneous rocks and crustal growth models. Journal of the Geological Society of London 151, 855–868.
Taylor, S.R., McLennan, S.M., 1985. The continental crust: its composition and evolution. Oxford Press Blackwell 1–312.
Thrane, K., 2002. Relationships between Archaean and Palaeoproterozoic crystalline basement complexes in the southern part of the East Greenland Caledonides: an ion microprobe study. Precambrian Research 113, 19–42.
Trap, P., Faure, M., Lin, W., Bruguier, O., Monie, P., 2007. Late Paleoproterozoic (1900–1800 Ma) nappe stacking and polyphase deformation in the Hengshan–Wutaishan area: implications for the understanding of the Trans-North-China Belt, North China Craton. Precambrian Research 156, 85–106.
Vervoort, J.D., Blichert-Toft, J., 1999. Evolution of the depleted mantle; Hf isotope evidence from juvenile rocks through time. Geochimica et Cosmochimica Acta 63, 533–556.
Wan, Y.S., Liu, D.Y., Wang, S.J., Dong, C.Y., Yang, E.X., Wang, W., Zhou, H.Y., Du, L.L., Yin, X.Y., Xie, H.Q., Ma, M.Z., 2010. Juvenile magmatism and crustal recycling at the end of Neoarchean in western Shandong province, north China Craton: evidence from SHRIMP zircon dating. American Journal of Science 310, 1503–1552.
Wan, Y.S., Liu, D.Y., Wang, S.J., Yang, E.X., Wang, W., Dong, C.Y., Zhou, H.Y., Du, L.L., Yang, Y.H., Diwu, C.R., 2011. 2.7 Ga juvenile crust formation in the North China Craton (Taishan–Xintai area, western Shandong Province): further evidence of an understated event from U–Pb dating and Hf isotopic composition of zircon. Precambrian Research 186, 169–180.
Wan, Y.S., Liu, D.Y., Nutman, A., Zhou, H.Y., Dong, C.Y., Yin, X.Y., Ma, M.Z., 2012a. Multiple 3.8–3.1 Ga tectono-magmatic events in a newly discovered area of ancient rocks (the Shengousi Complex), Anshan, North China Craton. Journal of Asian Earth Sciences 54–55, 18–30.
Wan, Y.S., Wang, S.J., Liu, D.Y., Wang, W., Kröner, A., Dong, C.Y., Yang, E.X., Zhou, H.Y., Xie, H.Q., Ma, M.Z., 2012b. Redefinition of depositional ages of Neoarchean supracrustal rocks in western Shandong Province, China: SHRIMP U–Pb zircon dating. Gondwana Research 21, 768–784.
Wan, Y.S., Dong, C.Y., Liu, D.Y., Kröner, A., Yang, C.H., Wang, W., Du, L.L., Xie, H.Q., Ma, M.Z., 2012c. Zircon ages and geochemistry of late Neoarchean syenogranites in the North China Craton: a review. Precambrian Research 222–223, 265–289.
Wang, Y.J., Zhang, Y.Z., Zhao, G.C., Fan, W.M., Xia, X.P., Zhang, F.F., Zhang, A.M., 2009. Zircon U–Pb geochronological and geochemical constraints on the petrogenesis of the Taishan sanukitoids (Shandong): implications for Neoarchean subduction in the Eastern Block, North China Craton. Precambrian Research 174, 273–286.
Watkins, J., Clemens, J., Treloar, P., 2007. Archaean TTGs as sources of younger granitic magmas: melting of sodic metatonalites at 0.6–1.2 GPa. Contributions to Mineralogy and Petrology 154, 91–110.
Weaver, B.L., 1991. The origin of ocean island basalt end-member compositions: trace element and isotopic constraints. Earth and Planetary Science Letters 104, 381–397.
Wilde, S.A., Valley, J.W., Peck, W.H., Graham, C.M., 2001. Evidence from detrital zircons for the existence of continental crust and oceans on the Earth 4.4 Gyr ago. Nature 409, 175–178.
Wilde, S.A., Cawood, P.A., Wang, K.Y., Nemchin, A., 2005. Granitoid evolution in the late Archean Wutai Complex, North China Craton. Journal of Asian Earth Sciences 24, 597–613.
Wilde, S.A., Valley, J.W., Kita, N.T., Cavosie, A.J., Liu, D.Y., 2008. SHRIMP U–Pb and Cameca 1280 oxygen isotope results from ancient detrital zircons in the Caozhuang quartzite, Eastern Hebei, North China Craton: evidence for crustal recycling 3.8 Ga ago. American Journal of Science 308, 185–199.
Winchester, J.A., Floyd, P.A., 1977. Geochemical discrimination of different magma series and their differentiation products using immobile elements. Chemical Geology 20, 325–343.
Woodhead, J.D., Hergt, J.M., Shelley, M., Eggins, S., Kemp, R., 2004. Zircon Hf-isotope analysis with an excimer laser, depth profiling, ablation of complex geometries, and concomitant age estimation. Chemical Geology 209, 121–135.
Wu, J.S., Geng, Y.S., Shen, Q.H., Wan, Y.S., Liu, D.Y., Song, B., 1998. Archean Geology Characteristics and Tectonic Evolution of China–Korean Paleocontinent. Geological Publishing House, Beijing, pp. 1–212 (in Chinese).
Wu, F.Y., Yang, J.H., Liu, X.M., Li, T.S., Xie, L.W., Yang, Y.H., 2005a. Hf isotopes of the 3.8 Ga zircons in eastern Hebei Province, China: implications for early crustal evolution of the North China Craton. Chinese Science Bulletin 50, 2473–2480.

Wu, F.Y., Zhao, G.C., Wilde, S.A., Sun, D., 2005b. Nd isotopic constraints on crustal formation in the North China Craton. Journal of Asian Earth Sciences 24, 523–545.
Wu, F.Y., Zhang, Y.B., Yang, J.H., Xie, L.W., Yang, Y.H., 2008. Zircon U–Pb and Hf isotopic constraints on the Early Archean crustal evolution in Anshan of the North China Craton. Precambrian Research 167, 339–362.
Wyman, D.A., Kerrich, R., Polat, A., 2002. Assembly of Archean cratonic mantle lithosphere and crust: plume–arc interaction in the Abitibi–Wawa subduction–accretion complex. Precambrian Research 115, 37–62.
Xia, X.P., Sun, M., Zhao, G.C., Luo, Y., 2006a. LA-ICP-MS U–Pb geochronology of detrital zircons from the Jining Complex, North China Craton and its tectonic significance. Precambrian Research 144, 199–212.
Xia, X.P., Sun, M., Zhao, G.C., Wu, F.Y., Xu, P., Zhang, J.H., Luo, Y., 2006b. U–Pb and Hf isotopic study of detrital zircons from the Wulashan khondalites: constraints on the evolution of the Ordos Terrane, Western Block of the North China Craton. Earth and Planetary Science Letters 241, 581–593.
Xia, X.P., Sun, M., Zhao, G.C., Wu, F.Y., Xu, P., Zhang, J.S., 2008. Paleoproterozoic crustal growth events in the Western Block of the North China Craton: evidence from detrital zircon Hf and whole rock Sr–Nd isotopes of the khondalites in the Jining Complex. American Journal of Science 308, 304–327.
Xia, X.P., Sun, M., Zhao, G.C., Wu, F.Y., Xu, P., Zhang, J.S., 2009. Detrital zircon U–Pb age and Hf isotope study of the khondalite in Trans-North China Orogen and its tectonic significance. Geological Magazine 146, 701–716.
Xia, X.P., Sun, M., Zhao, G.C., Wang, Y.J., 2011. Quasi-simultaneous determination of U–Pb and Hf isotope compositions of zircon by excimer laser-ablation multiple-collector ICPMS. Journal of Analytical Atomic Spectrometry 26, 1868–1871.
Xu, H.F., Dong, Y.J., Shi, R.H., Jin, R.M., Shen, K., Li, X.G., 1992. The Granitoid–Greenstone Belts of Western Shangdong. Geological Publishing House, Beijing, pp. 1–83 (in Chinese with English abstract).
Yang, J.H., Wu, F.Y., Wilde, S.A., Zhao, G.Z., 2008. Petrogenesis and geodynamics of Late Archean magmatism in eastern Hebei, eastern North China Craton: geochronological, geochemical and Nd–Hf isotopic evidence. Precambrian Research 167, 125–149.
Ye, H.M., Li, X.H., Li, Z.X., Zhang, C.L., 2008. Age and origin of high Ba–Sr appinite–granites at the northwestern margin of the Tibet Plateau: implications for early Paleozoic tectonic evolution of the Western Kunlun orogenic belt. Gondwana Research 13, 126–138.
Yin, C.Q., Zhao, G.C., Sun, M., Xia, X.P., Wei, C.J., Zhou, X.W., Leung, W.H., 2009. LA-ICP-MS U–Pb zircon ages of the Qianlishan Complex: constrains on the evolution of the Khondalite Belt in the Western Block of the North China Craton. Precambrian Research 174, 78–94.
Yin, C.Q., Zhao, G.C., Guo, J.H., Sun, M., Zhou, X.W., Zhang, J., Xia, X.P., Liu, C.H., 2011. U–Pb and Hf isotopic study of zircons of the Helanshan Complex: constrains on the evolution of the Khondalite Belt in the Western Block of the North China Craton. Lithos 122, 25–38.
Yogodzinski, G.M., Volynets, O.N., Koloskov, A.V., Seliverston, N.I., Matvenkov, V.V., 1994. Magnesian andesites and the subduction component in a strongly calc-alkaline series at Piip Volcano, far Western Aleutians. Journal of Petrology 35, 163–204.
Yogodzinski, G.M., Kay, R.W., Bolynets, O.N., Koloskov, A.V., Kay, S.M., 1995. Magnesian andesite in the western Aleutian Komandorsky region: implications for slab melting and processes in the mantle wedge. Geological Society of America Bulletin 107, 505–519.
Zhang, J., Zhao, G.C., Sun, M., Wilde, S.A., Li, S.Z., Liu, S.W., 2006. High-pressure mafic granulites in the Trans-North China Orogen: tectonic significance and age. Gondwana Research 9, 349–362.
Zhang, J., Zhao, G.C., Li, S.Z., Sun, M., Liu, S.W., Wilde, S.A., Kröner, A., Yin, C.Q., 2007. Deformation history of the Hengshan Complex: implications for the tectonic evolution of the Trans-North China Orogen. Journal of Structural Geology 29, 933–949.
Zhang, J., Zhao, G.C., Li, S.Z., Sun, M., Wilde, S.A., Liu, S.W., Kroner, A., Yin, C.Q., 2009. Polyphase deformation of the Fuping Complex, Trans-North China Orogen: structures, SHRIMP U–Pb zircon ages and tectonic implications. Journal of Structural Geology 31, 177–193.
Zhao, G.C., 2009. Metamorphic evolution of major tectonic units in the basement of the North China Craton: key issues and discussion. Acta Petrologica Sinica 25, 1772–1792.
Zhao, G.C., Wilde, S.A., Cawood, P.A., Lu, L.Z., 1998. Thermal evolution of the Archaean basement rocks from the eastern part of the North China Craton and its bearing on tectonic setting. International Geology Review 40, 706–721.
Zhao, G.C., Wilde, S.A., Cawood, P.A., Lu, L.Z., 1999a. Thermal evolution of two types of mafic granulites from the North China craton: implications for both mantle plume and collisional tectonics. Geological Magazine 136, 223–240.
Zhao, G.C., Wilde, S.A., Cawood, P.A., Lu, L.Z., 1999b. Tectonothermal history of the basement rocks in the western zone of the North China Craton and its tectonic implications. Tectonophysics 310, 37–53.
Zhao, G.C., Cawood, P.A., Wilde, S.A., Lu, L.Z., 2000. Metamorphism of basement rocks in the Central Zone of the North China Craton: implications for Paleoproterozoic tectonic evolution. Precambrian Research 103, 55–88.
Zhao, G.C., Wilde, S.A., Cawood, P.A., Sun, M., 2001. Archean blocks and their boundaries in the North China Craton: lithological, geochemical, structural and P–T path constraints and tectonic evolution. Precambrian Research 107, 45–73.
Zhao, G.C., Sun, M., Wilde, S.A., 2002. Major tectonic units of the North China Craton and their Paleoproterozoic assembly. Science in China Series D: Earth Sciences 32, 538–549 (in Chinese).
Zhao, G.C., Sun, M., Wilde, S.A., 2003. Major tectonic units of the North China Craton and their Paleoproterozoic assembly. Science in China Series D: Earth Sciences 46, 23–38.
Zhao, G.C., Sun, M., Wilde, S.A., Li, S.Z., 2005. Late Archean to Paleoproterozoic evolution of the North China Craton: key issues revisited. Precambrian Research 136, 177–202.
Zhao, G.C., Sun, M., Wilde, S.A., Li, S.Z., Liu, S.W., Zhang, J., 2006. Composite nature of the North China Granulite-Facies Belt: tectonothermal and geochronological constraints. Gondwana Research 9, 337–348.
Zhao, G.C., Kroner, A., Wilde, S.A., Sun, M., Li, S.Z., Li, X.P., Zhang, J., Xia, X.P., He, Y.H., 2007. Lithotectonic elements and geological events in the Hengshan–Wutai–Fuping belt: a synthesis and implications for the evolution of the Trans-North China Orogen. Geological Magazine 144, 753–775.
Zhao, G.C., Wilde, S.A., Sun, M., Guo, J.H., Kroner, A., Li, S.Z., Li, X.P., Wu, C.M., 2008a. SHRIMP U–Pb zircon geochronology of the Huai'an Complex: constraints on Late Archean to Paleoproterozoic crustal accretion and collision of the Trans-North China Orogen. American Journal of Science 308, 270–303.
Zhao, G.C., Wilde, S.A., Sun, M., Li, S.Z., Li, X.P., Zhang, J., 2008b. SHRIMP U–Pb zircon ages of granitoid rocks in the Lüliang Complex: implications for the accretion and evolution of the Trans-North China Orogen. Precambrian Research 160, 213–226.
Zhao, G.C., Wilde, S.A., Guo, J.H., Cawood, P.A., Sun, M., Li, X.P., 2010. Single zircon grains record two continental collisional events in the North China craton. Precambrian Research 177, 266–276.
Zhao, G.C., Cawood, P.A., Li, S.Z., Wilde, S.A., Sun, M., Zhang, J., He, Y.H., Yin, C.Q., 2012. Amalgamation of the North China Craton: key issues and discussion. Precambrian Research 222–223, 55–76.
Zheng, J.P., Griffin, W.L., O'Reilly, S.Y., Zhao, J.H., Wu, Y.B., Liu, G.L., Pearson, N., Zhang, M., Ma, C.Q., Zhang, Z.H., Yu, C.M., Su, Y.P., Tang, H.Y., 2009. Neoarchean (2.7–2.8 Ga) accretion beneath the North China Craton: U–Pb age, trace elements and Hf isotopes of zircons in diamondiferous kimberlites. Lithos 112, 188–202.
Zhou, X.W., Zhao, G.C., Wei, C.J., Geng, Y.S., Sun, M., 2008. Metamorphic evolution and Th–U–Pb zircon and monazite geochronology of high-pressure pelitic granulites in the Jiaobei massif of the North China Craton. American Journal of Science 308, 328–350.
Zhou, X.W., Zhao, G.C., Geng, Y.S., 2010. Helanshan high-pressure pelitic granulites: petrological evidence for collision event in the Western Block of the North China Craton. Acta Petrologica Sinica 26, 2113–2121.